applied sciences

MDPI

Article

Design Procedure for Motion Profiles with Sinusoidal Jerk for Vibration Reduction

Yi Fang [1], Guo-Niu Zhu [2,*], Yudi Zhao [1] and Chaochen Gu [1,*]

1 School of Electronic Information and Electrical Engineering, Shanghai Jiao Tong University, Shanghai 200240, China; apocalypse@sjtu.edu.cn (Y.F.); yudizhao@sjtu.edu.cn (Y.Z.)
2 Academy for Engineering and Technology, Fudan University, Shanghai 200433, China
* Correspondence: guoniu_zhu@fudan.edu.cn (G.-N.Z.); jacygu@sjtu.edu.cn (C.G.)

Abstract: High-speed motions performed by industrial machines can induce severe vibrations that degrade the positioning accuracy and efficiency. To address this issue, this paper proposes a novel motion profile design method utilizing a sinusoidal jerk model to generate fast and smooth motions with low vibrations. The expressions for the acceleration, velocity, and displacement were obtained through successive integrations of the continuous jerk profile. A minimum-time solution with actuator limits was formulated based on an analysis of the critical constraint conditions. Differing from previous studies, the current study introduces an analytical optimization procedure for the profile parameters to minimize both the motion duration and excitation frequency contents corresponding to the system pole. By examining the correlation between the input motion profiles and system responses, the conditions for vibration elimination were identified, highlighting the significance of specific time intervals in controlling the vibration amplitude. Numerical and experimental studies were conducted to validate the effectiveness of the proposed method. The comparative results illustrate that this method outperforms existing baseline techniques in terms of smoothness and vibration attenuation. The residual-vibration level and settling time are significantly reduced with the optimized sinusoidal jerk profile, even in the presence of modeling errors, contributing to higher productivity.

Keywords: motion profile; vibration reduction; trajectory optimization; residual vibration; sinusoidal jerk; motion control

Citation: Fang, Y.; Zhu, G.-N.; Zhao, Y.; Gu, C. Design Procedure for Motion Profiles with Sinusoidal Jerk for Vibration Reduction. *Appl. Sci.* **2023**, *13*, 13320. https://doi.org/10.3390/app132413320

Academic Editors: Renato Vidoni, Lorenzo Scalera and Andrea Giusti

Received: 2 November 2023
Revised: 11 December 2023
Accepted: 14 December 2023
Published: 17 December 2023

1. Introduction

Faster and more accurate movements are generally required to improve the productivity and quality of manufacturing, which presents a challenge for the control systems of automated machines in various industrial applications, including assembly, painting, welding, machining, quality inspection, and material handling [1–3]. In fact, in many automation tasks, the transfer time often constitutes a significant portion of the overall cycle time. However, high-speed motions tend to induce unwanted vibrations that can degrade the positioning time and accuracy. Consequently, motion profile design for achieving rapid movements with low vibrations has emerged as a motivating and valuable research topic in the field of control engineering [4,5]. Motion profiles define the temporal evolution of the reference position, velocity, and acceleration that a machine should follow to accomplish a specific task. A well-designed motion profile can effectively provide benefits in terms of cycle time reduction, vibration lessening, and precision enhancement, ultimately contributing to improved product quality, increased overall process efficiency, and a prolonged machine life. Moreover, it enables the avoidance of energy dissipation caused by mechanical vibrations; thus, the conversion rate of electric energy into actuation energy can be improved, saving energy consumption [6,7].

Aiming to achieve faster movements, machines may be expected to work within their physical limitations, causing undesired adverse impacts that compromise their performances. It is widely known that, for given limits on the velocity and force/torque, the trapezoidal velocity profile, which consists of constant acceleration and deceleration in the initial and final phases, respectively, while maintaining maximum velocity in the intermediate phase, minimizes the motion completion time [8,9]. To date, this profile remains a fundamental choice that is broadly employed in production equipment, such as manipulators or machine tools, due to its simplicity. Heo et al. [10] proposed a profile generator based on a cascaded P-PI position controller and dynamic-range limiters to remove the steady-state error. A closed-form parameter-tuning approach for the energy-saving velocity profiles of servomotor systems was investigated in [11] by formulating a quasi-convex optimization problem. The main limitation is that discontinuities in acceleration tend to stimulate resonant modes, leading to mechanical structure damage and additional time consumption for motion-induced vibration dissipation at the desired position [12]. The adoption of more lightweight and flexible structures with low stiffness in modern industry exacerbates this issue [13]. Though some works have attempted to optimize the acceleration time to minimize the residual vibrations [14–16], the presence of high-frequency components in the trapezoidal profile necessitates a wide servo bandwidth to ensure tracking accuracy.

This dilemma has driven researchers to devise more sophisticated and precise motion profiles that satisfy the desired task specifications while respecting the system's limitations and optimization constraints [17]. As a consequence, the S-curve profile has been developed to yield smoother motions that are easy to implement [18,19]. By replacing the step acceleration pulses with ramps, this profile exhibits a finite distribution of jerk (the time derivative of acceleration) over a period of time. Numerous studies have shown that S-curve profiles offer advantages in minimizing undesirable effects, such as vibrations, overshoot, actuator stress, and component wear, when compared to trapezoidal velocity profiles [20–22]. An algorithm to generate a seven-segment velocity profile is developed in [23] for motion control in a hybrid electronic platform. Meckl et al. [24] optimized the ramp-up time of S-curve profiles based on the frequency content of the force input to minimize the response time and residual vibrations. Liu et al. [25] proposed an optimization model to achieve the time-optimal asymmetrical S-curve velocity scheduling of a specified end-effector path with kinematic constraints. However, the limited jerk employed in these profiles is accompanied by sudden transitions at the switching instances of segments, which are associated with high-frequency content.

To further dampen vibrations, considerable research efforts have been devoted to attaining smooth changes in jerk. A representative idea of defining such a motion law is based on higher-order polynomials and trigonometric functions [26–29]. Lambrecht et al. [30] suggested a fourth-order trajectory-planning algorithm with feedforward control under given physical bounds for electromechanical motion systems. Da Rocha et al. [31] developed a smooth, real-time, snap-bounded profile generation technique based on an embedded-system platform. The experimental results showed that the snap-constrained method effectively reduces the tracking error when compared to the seven-segment and trapezoidal velocity methods. Bilal et al. [32] employed the concatenation of quintic polynomials to provide a bounded and continuous jerk point-to-point trajectory for the vibration control of a flexible-joint manipulator with parametric uncertainties. However, the complexity becomes significant as the number of profile segments increases, presenting a challenge for real-time applications. In some cases, the utilization of a numerical method is necessary, which may fail to obtain a feasible solution or become stuck in local convergence due to the selection of an inappropriate initial solution. To avoid the excessive computational burden for the controller brought on by high-degree polynomials, Li et al. [33] present a low-vibration motion profile generation scheme using a level-shifted sinusoidal waveform to design the acceleration profile for high-speed positioning. Simulation and experimental studies have demonstrated that their method achieves remarkably lower residual vibrations relative to the conventional trapezoidal profile and S-curve profile. The main limitation of this scheme is its incompleteness in addressing special cases, rendering it inapplicable under certain physical constraints. Perumaal et al. [34] studied a jerk-bounded trigonometric S-curve trajectory planner based on a three-phase sine jerk motion profile for the pick-and-place operations of a six-DOF robotic manipulator. However, the study does not guarantee the fulfillment of specified kinematic constraints and time optimality. More recently, Valente et al. [35], using the same profile, adopted a multivariable time optimization method to expand the range of feasible solutions for achieving the shortest running time. Wu et al. [36] utilized a locally asymmetrical jerk profile to establish smooth and time-optimal point-to-point trajectories for industrial robots. In [37], a trigonometric feed-rate-scheduling algorithm is introduced to enable the continuous velocity, acceleration, and jerk control of the parametric interpolation, which reduces undesirable vibrations in high-speed and high-accuracy machining. However, most of these studies mainly dealt with the generation of trajectories with time optimality under physical limits, while comprehensive quantitative analyses of the influence of the profile parameters on the vibration responses were neglected. To ensure that machines produce rapid and precise movements, the optimization of the profile parameters adapted to the vibration behavior is of significance.

Motivated by these early works, the main purpose of this paper is to propose a novel motion profile design method characterized by a continuous sinusoidal jerk model for the vibration mitigation of high-speed industrial machines. As a consequence, a smooth motion is ensured to reduce the positioning time and error, leading to improved productivity and quality. The contributions of this work are as follows: (1) First, a closed-form solution for the minimum-time sinusoidal jerk profile was derived, enabling the full exploitation of the actuator limits based on profile type evaluation. The critical kinematic values were identified to classify the proposed model into four specific types according to the input displacement and actuator limits. (2) Furthermore, a quantitative investigation of the relationship between the profile parameters and the response characteristics was performed to identify the vibration suppression conditions. The analysis revealed that the vibration level is primarily influenced by the proportion between specific time intervals and the natural period, rather than lower jerk values. (3) Finally, an optimization procedure was suggested to obtain the time–frequency-optimal sinusoidal jerk profile that minimizes the motion duration while considering the desired vibration cancellation and robustness constraints without violating the physical limits. Numerical and experimental tests were carried out to demonstrate the effectiveness of the proposed method.

The rest of this paper is organized as follows: Section 2 begins with a brief review of the S-curve profile, followed by the definition and analytical expressions of the sinusoidal jerk profile. The minimum-time solution subject to the actuator limits is described in Section 3. After that, the characteristics of motion-induced residual vibrations are analyzed, and the optimization strategy of the profile parameters for vibration suppression is also developed. Then, Section 4 presents the kinematic and dynamic simulation results, assessing the vibrations induced by different motion profiles. Section 5 reports the experimental results to evaluate the performance of the optimized profile in comparison with other baseline methods on a motion stage. Finally, the conclusions and future work are drawn up in Section 6.

2. General Formulation of Motion Profiles

2.1. Review of Seven-Segment S-Curve Profile

To avoid acceleration discontinuities, the S-curve velocity profile, also known as the third-order motion profile, has been extensively studied and applied in recent years. Due to the characteristic of finite jerk spread over time, this profile enables the generation of smooth motions with small residual vibrations. For the rest-to-rest motion, a complete profile consists of seven symmetrically distributed segments, in which the jerk remains constant at zero or its peak value, as shown in Figure 1, where t_i, $i = 0, 1, \ldots, 7$ are the time boundaries of each segment; T_1, T_2, and T_3 represent the time periods for the constant jerk segment, constant acceleration segment, and constant velocity segment, respectively. The first three segments constitute the acceleration phase, while the last three segments constitute the deceleration phase.

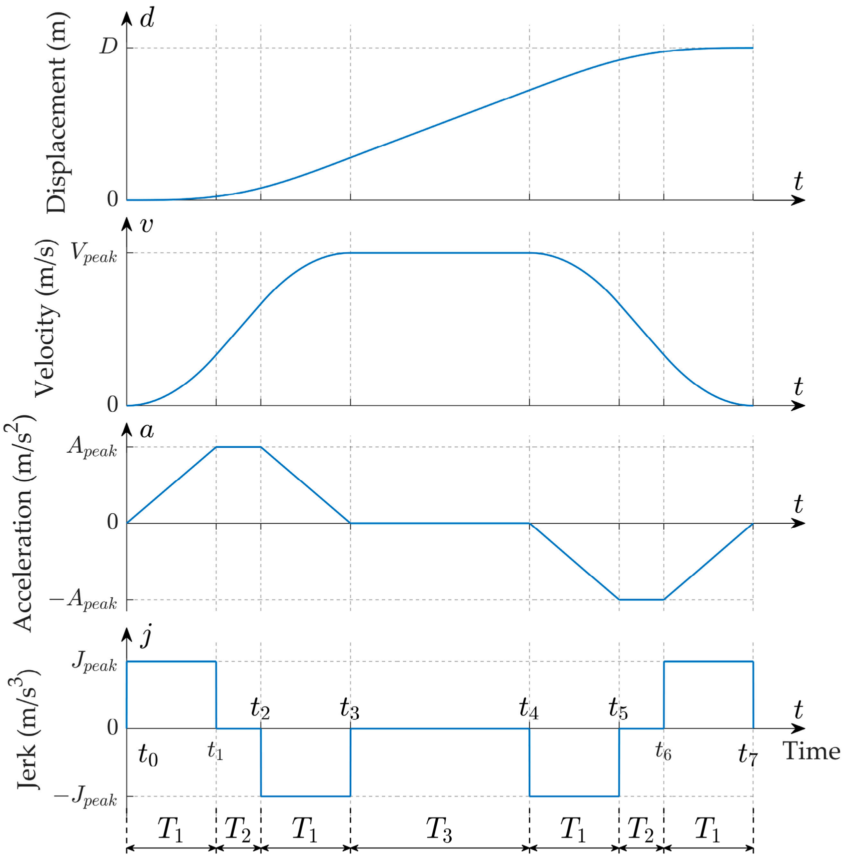

Figure 1. Seven-segment S-curve motion profile.

Let J_{peak} denote the peak value of the jerk; then, the jerk profile can be expressed as follows:

$$j(t) = \begin{cases} J_{peak}, & t_0 \leq t < t_1 \\ 0, & t_1 \leq t < t_2 \\ -J_{peak}, & t_2 \leq t < t_3 \\ 0, & t_3 \leq t < t_4 \\ -J_{peak}, & t_4 \leq t < t_5 \\ 0, & t_5 \leq t < t_6 \\ J_{peak}, & t_6 \leq t < t_7 \end{cases}. \tag{1}$$

As a result, the acceleration changes linearly, reaching its maximum magnitude in the second and sixth segments. It takes a trapezoidal form during the acceleration phase $[t_0,\ t_3]$ and an inverse trapezoidal form during the deceleration phase $[t_4,\ t_7]$. In the intermediate phase, the velocity maintains its maximum value, while the acceleration turns to zero. Accordingly, the displacement curve is depicted by connected polynomial segments up to the third order. However, step jumps in the jerk degrade the performance to some extent. More details about this motion profile can be referred to in [38–40].

2.2. Mathematical Expressions of Sinusoidal Jerk Profile

To mitigate the rate of change in acceleration, the rectangular jerk pulses in segments 1, 3, 5, and 7 of the S-curve profile are replaced by sinusoidal waveforms to ensure jerk continuity. Similarly, the sinusoidal jerk profile consists of the acceleration phase, cruise phase, and deceleration phase, which can be further divided into seven segments, as shown in Figure 2. T_1, T_2, and T_3 represent the time periods for the sinusoidal jerk segment, constant acceleration segment, and constant velocity segment, respectively. Under the assumption that the profile has a symmetrical shape with the same acceleration and deceleration time, the time periods are defined as follows: $T_1 = t_1 - t_0 = t_3 - t_2 = t_5 - t_4 = t_7 - t_6$, $T_2 = t_2 - t_1 = t_6 - t_5$, and $T_3 = t_4 - t_0$. Consequently, the motion profile is fully defined by these three time parameters and the peak jerk parameter. The total duration of the motion profile is calculated as $T_f = 4T_1 + 2T_2 + T_3$.

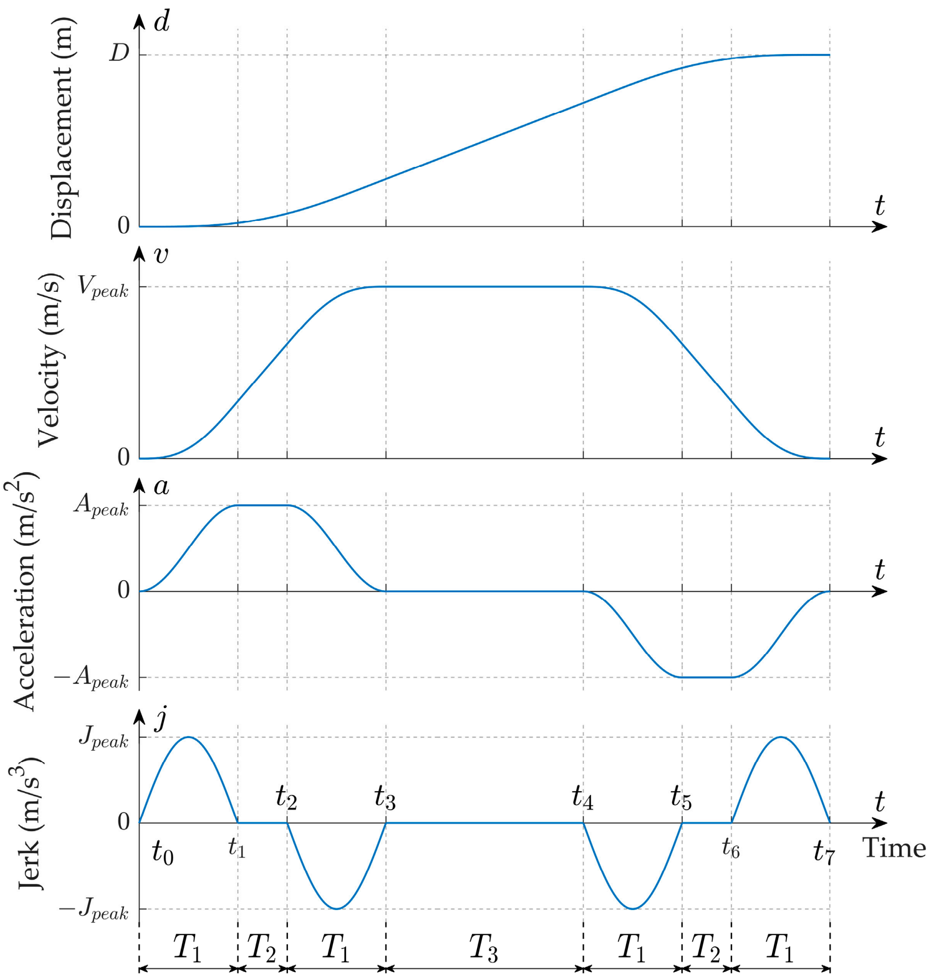

Figure 2. General sinusoidal jerk motion profile (Type 1).

The expression of the jerk profile is described as follows:

$$j(t) = \begin{cases} J_{peak} \sin\left(\frac{\pi}{T_1}(t - t_0)\right), & t_0 \leq t < t_1 \\ 0, & t_1 \leq t < t_2 \\ -J_{peak} \sin\left(\frac{\pi}{T_1}(t - t_2)\right), & t_2 \leq t < t_3 \\ 0, & t_3 \leq t < t_4 \, , \\ -J_{peak} \sin\left(\frac{\pi}{T_1}(t - t_4)\right), & t_4 \leq t < t_5 \\ 0, & t_5 \leq t < t_6 \\ J_{peak} \sin\left(\frac{\pi}{T_1}(t - t_6)\right), & t_6 \leq t < t_7 \end{cases} \quad (2)$$

where J_{peak} stands for the peak jerk value during the sinusoidal jerk segment. The corresponding mathematical expressions for the acceleration, velocity, and position profiles can then be derived by sequentially integrating Equation (2):

$$\begin{cases} a(t) = a(t_i) + \int_{t_i}^{t} j(t)dt \\ v(t) = v(t_i) + \int_{t_i}^{t} a(t)dt \\ d(t) = d(t_i) + \int_{t_i}^{t} v(t)dt \end{cases}. \quad (3)$$

Note that the peak acceleration is attained at the end of the sinusoidal jerk segment and is maintained during the segment $[t_1,\ t_2]$:

$$A_{peak} = a(t_1) = \int_{t_0}^{t_1} J_{peak} \sin\left(\frac{\pi}{T_1}(t - t_0)\right)dt = \frac{2J_{peak}T_1}{\pi}. \quad (4)$$

Consequently, the expression of the acceleration profile can be written as follows:

$$a(t) = \begin{cases} \frac{A_{peak}}{2}\left(1 - \cos\frac{\pi}{T_1}(t - t_0)\right), & t_0 \le t < t_1 \\ A_{peak}, & t_1 \le t < t_2 \\ \frac{A_{peak}}{2}\left(1 + \cos\frac{\pi}{T_1}(t - t_2)\right), & t_2 \le t < t_3 \\ 0, & t_3 \le t < t_4 \\ -\frac{A_{peak}}{2}\left(1 - \cos\frac{\pi}{T_1}(t - t_4)\right), & t_4 \le t < t_5 \\ -A_{peak}, & t_5 \le t < t_6 \\ -\frac{A_{peak}}{2}\left(1 + \cos\frac{\pi}{T_1}(t - t_6)\right), & t_6 \le t < t_7 \end{cases}. \quad (5)$$

Likewise, the peak velocity is reached at the end of the acceleration phase and remains constant during the segment $[t_3,\ t_4]$, which can be readily determined using geometric principles due to symmetry:

$$V_{peak} = v(t_3) = A_{peak}(T_1 + T_2) = \frac{2J_{peak}T_1}{\pi}(T_1 + T_2). \quad (6)$$

The expression of the velocity profile is given as follows:

$$v(t) = \begin{cases} \frac{A_{peak}}{2}\left((t - t_0) - \frac{T_1}{\pi}\sin\frac{\pi}{T_1}(t - t_0)\right), & t_0 \le t < t_1 \\ \frac{A_{peak}T_1}{2} + A_{peak}(t - t_1), & t_1 \le t < t_2 \\ A_{peak}\left(\frac{T_1}{2} + T_2\right) + \frac{A_{peak}}{2}(t - t_2) + \frac{A_{peak}T_1}{2\pi}\sin\frac{\pi}{T_1}(t - t_2), & t_2 \le t < t_3 \\ V_{peak}, & t_3 \le t < t_4 \\ V_{peak} - \frac{A_{peak}}{2}(t - t_4) + \frac{A_{peak}T_1}{2\pi}\sin\frac{\pi}{T_1}(t - t_4), & t_4 \le t < t_5 \\ V_{peak} - \frac{A_{peak}T_1}{2} - A_{peak}(t - t_5), & t_5 \le t < t_6 \\ \frac{A_{peak}T_1}{2} - \frac{A_{peak}}{2}(t - t_6) - \frac{A_{peak}T_1}{2\pi}\sin\frac{\pi}{T_1}(t - t_6), & t_6 \le t < t_7 \end{cases}. \quad (7)$$

The expression of the displacement profile is then found as follows:

$$d(t) = \begin{cases} \frac{A_{peak}}{4}(t-t_0)^2 + \frac{A_{peak}T_1{}^2}{2\pi^2}\cos\frac{\pi}{T_1}(t-t_0) - \frac{A_{peak}T_1{}^2}{2\pi^2}, & t_0 \le t < t_1 \\ \left(\frac{1}{4}-\frac{1}{\pi^2}\right)A_{peak}T_1{}^2 + \frac{A_{peak}T_1}{2}(t-t_1) + \frac{A_{peak}}{2}(t-t_1)^2, & t_1 \le t < t_2 \\ \left(\frac{1}{4}-\frac{1}{2\pi^2}\right)A_{peak}T_1{}^2 + \frac{A_{peak}T_1T_2}{2} + \frac{A_{peak}T_2{}^2}{2} + A_{peak}\left(\frac{T_1}{2}+T_2\right)(t-t_2) + \frac{A_{peak}}{4}(t-t_2)^2 - \frac{A_{peak}T_1{}^2}{2\pi^2}\cos\frac{\pi}{T_1}(t-t_2), & t_2 \le t < t_3 \\ V_{peak}\left(T_1+\frac{T_2}{2}\right) + V_{peak}(t-t_3), & t_3 \le t < t_4 \\ V_{peak}\left(T_1+\frac{T_2}{2}+T_3\right) + V_{peak}(t-t_4) - \frac{A_{peak}}{4}(t-t_4)^2 - \frac{A_{peak}T_1{}^2}{2\pi^2}\cos\frac{\pi}{T_1}(t-t_4) + \frac{A_{peak}T_1{}^2}{2\pi^2}, & t_4 \le t < t_5 \\ V_{peak}\left(2T_1+\frac{T_2}{2}+T_3\right) - \left(\frac{1}{4}-\frac{1}{\pi^2}\right)A_{peak}T_1{}^2 + V_{peak}(t-t_5) - \frac{A_{peak}T_1}{2}(t-t_5) - \frac{A_{peak}}{2}(t-t_5)^2, & t_5 \le t < t_6 \\ V_{peak}(2T_1+T_2+T_3) - \left(\frac{1}{4}-\frac{1}{2\pi^2}\right)A_{peak}T_1{}^2 + \frac{A_{peak}T_1}{2}(t-t_6) - \frac{A_{peak}}{4}(t-t_6)^2 + \frac{A_{peak}T_1{}^2}{2\pi^2}\cos\frac{\pi}{T_1}(t-t_6), & t_6 \le t < t_7 \end{cases}. \quad (8)$$

The terminal displacement at the end time of motion is represented as follows:

$$\begin{aligned} d_{end} &= d(t_7) = V_{peak}(2T_1+T_2+T_3) = A_{peak}(T_1+T_2)(2T_1+T_2+T_3) \\ &= \frac{2J_{peak}T_1}{\pi}(T_1+T_2)(2T_1+T_2+T_3) \end{aligned}. \quad (9)$$

To achieve fast, smooth, and precise movements, the profile parameters should be properly designed to minimize the motion duration while considering various constraint conditions, including the desired displacement, actuator specifications, residual-vibration suppression, and robustness against system uncertainties. Once these parameters are determined, the setpoints of the motion profile can be computed using the aforementioned expressions.

3. Parameter Design for Sinusoidal Jerk Profile

3.1. Minimum-Time Solution with Actuator Limits

Before addressing the optimization of the residual vibrations, we first consider the minimum-time solution with only the actuator limits. The motion profile design should ensure that the terminal displacement at the end of the movement is equal to the target moving distance. Moreover, the kinematic values during motion should stay within the physical limits. Given the desired displacement (D) and the maximum allowable values of the velocity ($V_{\max}$), acceleration ($A_{\max}$), and jerk ($J_{\max}$) imposed by the physical limitations of the actuators, the design constraint conditions are as follows: $d_{end} = D$, $\left|J_{peak}\right| \le J_{\max}$, $\left|A_{peak}\right| \le A_{\max}$, $\left|V_{peak}\right| \le V_{\max}$.

To minimize the motion duration, it is necessary for machines to take full advantage of the kinematic limits and maintain the saturated state for as long as possible. However, there are mutual restrictions among the constraint conditions so that it is not always possible for the motion profile to reach all the limit values. Specifically, the acceleration limit may not be achieved due to the tight limit on the velocity or a short moving distance, while the velocity limit may be unreachable due to the short distance traveled. Consequently, the corresponding constant acceleration and velocity segments may disappear, resulting in a motion profile with fewer than seven segments under different constraint conditions. According to the included segments, the profile model can be classified into four specific types, as illustrated in Figures 2 and 3.

By substituting the expressions of the peak kinematic values, the design constraints can be written as follows:

$$\begin{cases} \left|J_{peak}\right| \le J_{\max} \\ \left|\frac{2J_{peak}T_1}{\pi}\right| \le A_{\max} \\ \left|\frac{2J_{peak}T_1}{\pi}(T_1+T_2)\right| \le V_{\max} \\ \frac{2J_{peak}T_1}{\pi}(T_1+T_2)(2T_1+T_2+T_3) = D \end{cases}. \quad (10)$$

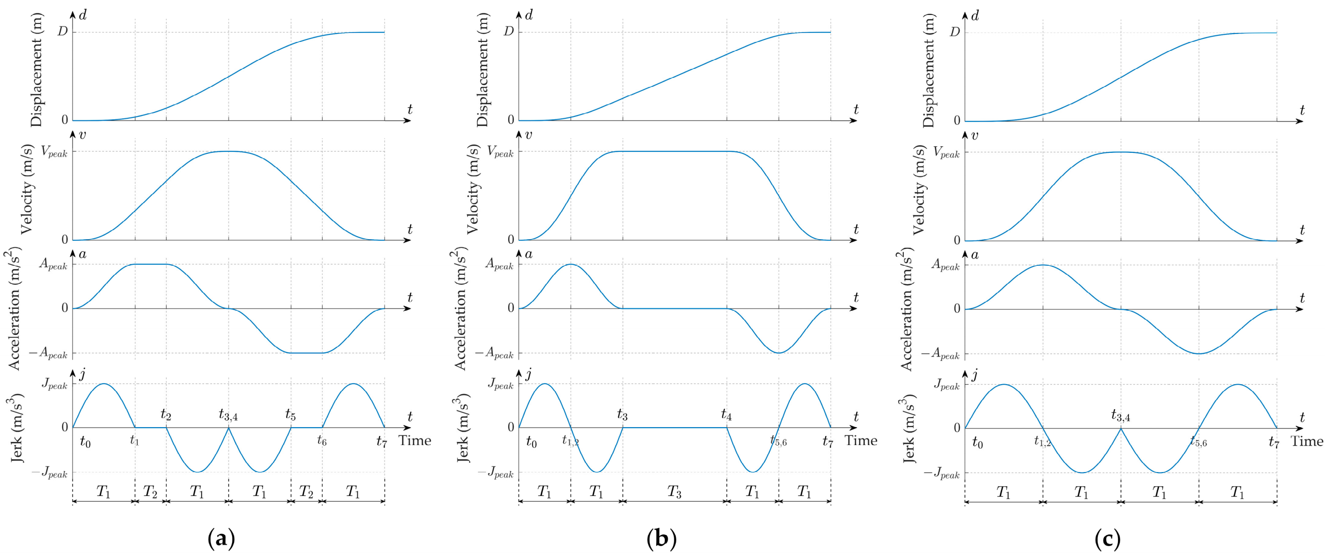

Figure 3. Different types of sinusoidal jerk motion profiles: (**a**) Type 2; (**b**) Type 3; (**c**) Type 4.

Note that the sinusoidal jerk segments must exist in the profile, enabling the jerk to consistently reach its limit value, namely, $J_{peak} = \text{sgn}(D)J_{\max}$ and $T_1 > 0$, $T_2 \geq 0$, $T_3 \geq 0$. Hence, the optimal value of T_1 that does not violate any constraints is as follows:

$$T_1 = \min\left\{\frac{\pi A_{\max}}{2J_{\max}}, \sqrt{\frac{\pi V_{\max}}{2J_{\max}}}, \sqrt[3]{\frac{\pi|D|}{2J_{\max}}}\right\}. \tag{11}$$

If $T_1 = \frac{\pi A_{\max}}{2J_{\max}}$, then T_1 is determined via the acceleration limit. The acceleration limit ($A_{\max}$) can be reached, namely, $A_{peak} = \text{sgn}(D)A_{\max}$; thus, we can continue to calculate T_2. The design constraints for T_2 are as follows:

$$\begin{cases} |A_{\max}(T_1 + T_2)| \leq V_{\max} \\ A_{\max}(T_1 + T_2)(2T_1 + T_2 + T_3) = |D| \end{cases}. \tag{12}$$

Therefore, the optimal value of T_2 that does not violate any constraints is as follows:

$$T_2 = \min\left\{\frac{V_{\max}}{A_{\max}} - T_1, -\frac{3T_1}{2} + \sqrt{\frac{T_1{}^2}{4} + \frac{|D|}{A_{\max}}}\right\}. \tag{13}$$

Two cases are distinguished here: If $T_2 = \frac{V_{\max}}{A_{\max}} - T_1$, then the moving distance is long enough for the motion profile to attain the velocity limit ($V_{\max}$). The motion profile belongs to Type 1 in Figure 2, with all seven segments present. Then, the time period for the constant velocity is calculated as follows:

$$T_3 = \frac{|D|}{V_{\max}} - 2T_1 - T_2; \tag{14}$$

otherwise, if $T_2 = -\frac{3T_1}{2} + \sqrt{\frac{T_1{}^2}{4} + \frac{|D|}{A_{\max}}}$, then the moving distance falls short of reaching the velocity limit ($V_{\max}$) within the motion profile. In this case, the motion profile belongs to Type 2, as shown in Figure 3a, where the constant velocity segment disappears (i.e., $T_3 = 0$). The peak velocity is determined using Equation (6) as $V_{peak} = A_{peak}(T_1 + T_2)$.

In addition, if $T_1 = \sqrt{\frac{\pi V_{\max}}{2J_{\max}}}$, this implies that T_1 is determined by the velocity limit. The motion profile is classified as Type 3, as shown in Figure 3b. The constant acceleration segments vanish due to the tight limit on the velocity (i.e., $T_2 = 0$), and T_3 can then be computed using Equation (14). The peak acceleration (A_{peak}) is lower than its maximum allowable value ($A_{\max}$) and is obtained using $A_{peak} = \frac{V_{peak}}{T_1}$.

Finally, if $T_1 = \sqrt[3]{\frac{\pi|D|}{2J_{\max}}}$, then T_1 is determined by the required displacement. The motion profile belongs to Type 4, as shown in Figure 3c, where only the sinusoidal jerk segments exist. Both the constant acceleration and velocity segments vanish due to the short moving distance (i.e., $T_2 = 0$, $T_3 = 0$). The peak acceleration and velocity are calculated using Equations (4) and (6) as $A_{peak} = \frac{2J_{peak}T_1}{\pi}$, $V_{peak} = \frac{2J_{peak}{T_1}^2}{\pi}$.

The solutions for the four profile types, along with the corresponding evaluation conditions, are summarized in Table 1.

Table 1. Complete minimum-time solutions for parameters of sinusoidal jerk profile.

	Type 1	Type 2	Type 3	Type 4
Critical Condition	$V_{\max} > \frac{\pi {A_{\max}}^2}{2J_{\max}}$, $\lvert D\rvert > \frac{\pi^2 {A_{\max}}^3}{4{J_{\max}}^2}$		$V_{\max} < \frac{\pi {A_{\max}}^2}{2J_{\max}}$,	$\lvert D\rvert < \frac{\pi^2 {A_{\max}}^3}{4{J_{\max}}^2}$,
	$\lvert D\rvert > \frac{{V_{\max}}^2}{A_{\max}} + \frac{\pi V_{\max} A_{\max}}{2J_{\max}}$	$\lvert D\rvert \le \frac{{V_{\max}}^2}{A_{\max}} + \frac{\pi V_{\max} A_{\max}}{2J_{\max}}$	$\lvert D\rvert > \sqrt{\frac{\pi {V_{\max}}^3}{2J_{\max}}}$	$\lvert D\rvert < \sqrt{\frac{\pi {V_{\max}}^3}{2J_{\max}}}$
T_1	$\frac{\pi A_{\max}}{2J_{\max}}$	$\frac{\pi A_{\max}}{2J_{\max}}$	$\sqrt{\frac{\pi V_{\max}}{2J_{\max}}}$	$\sqrt[3]{\frac{\pi\lvert D\rvert}{2J_{\max}}}$
T_2	$\frac{V_{\max}}{A_{\max}} - T_1$	$-\frac{3T_1}{2} + \sqrt{\frac{{T_1}^2}{4} + \frac{\lvert D\rvert}{A_{\max}}}$	0	0
T_3	$\left\lvert\frac{D}{V_{\max}}\right\rvert - 2T_1 - T_2$	0	$\left\lvert\frac{D}{V_{\max}}\right\rvert - 2T_1$	0

3.2. Analysis of Vibration Characteristics

The algorithm in the last subsection yields the solution that minimizes the execution time with the actuator limits. However, the quantitative consideration of the vibration response relating to the system modes is not incorporated into the motion profile design. The performance improvement in practice therefore appears to be almost exclusively due to smoothing. To investigate the relationship between the profile parameters and the vibration response, consider the simplified model in Figure 4, which includes a base, a mass (m), a spring with stiffness (k), and a damper (c). The dynamics of the system are described by the following expression:

$$-ky - c\dot{y} = m(\ddot{x} + \ddot{y}), \tag{15}$$

where x is the absolute position of the base and y is the relative position of the mass with respect to the base.

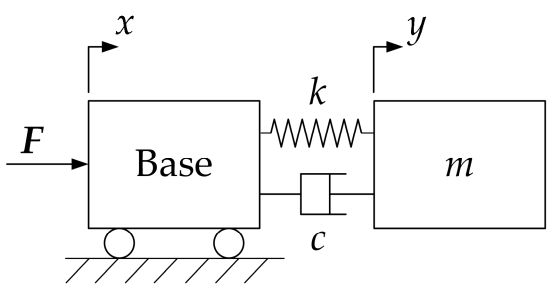

Figure 4. Modeling of flexible-motion system.

In this model, the base stands for the actuation system controlled by an input force, while the mass represents the mechanically linked structure that undergoes vibration. Thus, x and y serve as the reference input motion profile and dynamic response, respectively. Equation (15) can be written in Laplace form:

$$\frac{Y(s)}{X(s)} = \frac{-ms^2}{ms^2 + cs + k} = \frac{-s^2}{s^2 + 2\zeta\omega_n s + {\omega_n}^2}, \tag{16}$$

where $\omega_n = \sqrt{k/m}$ and $\zeta = c/\sqrt{4km}$ denote the undamped natural frequency and the damping ratio of the system, respectively. For a given reference input ($f(t)$), the dynamic response of the system can be calculated via the convolutional integral $y(t) = \int_0^\infty f(\tau)h(t-\tau)d\tau$, where $h(t)$ is the impulse response of the system, obtained from the inverse Laplace transform of Equation (16). Therefore, the dynamic motion-induced vibration response with the motion profile $x_1(t)$ is derived as follows:

$$\begin{aligned} y(t) &= -\int_0^t \ddot{x}(\tau)\frac{1}{\omega_n\sqrt{1-\zeta^2}}e^{-\zeta\omega_n(t-\tau)}\sin\left(\omega_n\sqrt{1-\zeta^2}(t-\tau)\right)d\tau \\ &= -\frac{1}{\omega_d}\int_0^t \ddot{x}(\tau)e^{-\zeta\omega_n(t-\tau)}\sin(\omega_d(t-\tau))d\tau \end{aligned}, \quad (17)$$

where $\omega_d = \omega_n\sqrt{1-\zeta^2}$ represents the damped natural frequency. For low-damped systems with $\zeta \approx 0$, the above expression is simplified as follows:

$$y(t) = -\frac{1}{\omega_d}\int_0^t \ddot{x}(\tau)\sin(\omega_d(t-\tau))d\tau. \quad (18)$$

By substituting Equation (5) into Equation (18), one can obtain the residual-vibration response after the completion of motion:

$$\begin{aligned} y_{res}(t) &= y(t|t \geq t_7) \\ &= -\frac{1}{\omega_d}\left[\begin{array}{l} \int_{t_0}^{t_1}\frac{A_{peak}}{2}\left(1-\cos\frac{\pi}{T_1}(\tau-t_0)\right)\sin(\omega_d(t-\tau))d\tau + \int_{t_1}^{t_2}A_{peak}\sin(\omega_d(t-\tau))d\tau \\ +\int_{t_2}^{t_3}\frac{A_{peak}}{2}\left(1+\cos\frac{\pi}{T_1}(\tau-t_2)\right)\sin(\omega_d(t-\tau))d\tau - \int_{t_4}^{t_5}\frac{A_{peak}}{2}\left(1-\cos\frac{\pi}{T_1}(\tau-t_4)\right)\sin(\omega_d(t-\tau))d\tau \\ -\int_{t_5}^{t_6}A_{peak}\sin(\omega_d(t-\tau))d\tau - \int_{t_6}^{t_7}\frac{A_{peak}}{2}\left(1+\cos\frac{\pi}{T_1}(\tau-t_6)\right)\sin(\omega_d(t-\tau))d\tau \end{array}\right]. \end{aligned} \quad (19)$$

After a series of mathematical operations involving integration by parts and the sum-to-product trigonometric identity, the above expression becomes the following:

$$y_{res}(t) = \frac{-4\pi^2 A_{peak}}{\omega_d{}^2\left(\pi^2-(\omega_d T_1)^2\right)}\cos\left(\frac{\omega_d T_1}{2}\right)\sin\left(\frac{\omega_d T_1}{2}+\frac{\omega_d T_2}{2}\right)\sin\left(\omega_d\left(T_1+\frac{T_2}{2}+\frac{T_3}{2}\right)\right)\cos\left(\omega_d\left((t-t_0)-\left(2T_1+T_2+\frac{T_3}{2}\right)\right)\right). \quad (20)$$

In order to eliminate the residual vibrations, the amplitude of the residual-vibration response must equal zero. Hence, settling $y_{res}(t) = 0$ yields the vibration suppression conditions:

$$\begin{cases} \pi^2-(\omega_d T_1)^2 \neq 0 \\ \cos\left(\frac{\omega_d T_1}{2}\right)\sin\left(\frac{\omega_d T_1}{2}+\frac{\omega_d T_2}{2}\right)\sin\left(\omega_d\left(T_1+\frac{T_2}{2}+\frac{T_3}{2}\right)\right) = 0 \end{cases}. \quad (21)$$

Without a loss of generality, the initial time (t_0) is assumed to be zero. Let $\mathbb{N}^+$ represent the set of positive integers. Then, the solution of (21) can be found as follows:

$$\text{C1}: T_1 = t_1 = \left(k_1+\frac{1}{2}\right)T_d, \quad k_1 \in \mathbb{N}^+, \quad (22)$$

$$\text{or C2}: T_1 + T_2 = t_2 = k_2 T_d, \quad k_2 \in \mathbb{N}^+, \quad (23)$$

$$\text{or C3}: 2T_1 + T_2 + T_3 = t_4 = k_3 T_d, \quad k_3 \in \mathbb{N}^+, \quad (24)$$

where $T_d = 2\pi/\omega_d$ is the vibration period of the system. According to the above analysis, if any one of the three conditions ((22), (23), or (24)) is satisfied, complete residual-vibration elimination can be achieved for an undamped system. Hereinafter, these conditions are denoted as C1, C2, and C3, respectively. Interestingly, although all of them result in a vibrationless stop, they display certain fundamentally distinct properties that impact the transient vibration during motion, as illustrated in Figure 5. These properties will be clarified in the following paragraphs. In a similar way, the dynamic response during the constant acceleration segments $[t_1,\ t_2]$ and $[t_5,\ t_6]$ can be derived as follows:

$$\begin{aligned} y(t|t_1 \leq t < t_2) &= -\frac{1}{\omega_d}\left[\int_{t_0}^{t_1} \frac{A_{peak}}{2}\left(1-\cos\frac{\pi}{T_1}(\tau-t_0)\right)\sin(\omega_d(t-\tau))d\tau + \int_{t_1}^{t} A_{peak}\sin(\omega_d(t-\tau))d\tau\right] \\ &= -\frac{A_{peak}}{\omega_d{}^2}\left[1-\frac{\pi^2}{\pi^2-(\omega_d T_1)^2}\cos\left(\frac{\omega_d T_1}{2}\right)\cos\left(\omega_d\left((t-t_0)-\frac{T_1}{2}\right)\right)\right] \end{aligned}, \quad (25)$$

$$\begin{aligned} y(t|t_5 \leq t < t_6) &= -\frac{1}{\omega_d}\left[\begin{array}{l} \int_{t_0}^{t_1} \frac{A_{peak}}{2}\left(1-\cos\frac{\pi}{T_1}(\tau-t_0)\right)\sin(\omega_d(t-\tau))d\tau + \int_{t_1}^{t_2} A_{peak}\sin(\omega_d(t-\tau))d\tau \\ +\int_{t_2}^{t_3} \frac{A_{peak}}{2}\left(1+\cos\frac{\pi}{T_1}(\tau-t_2)\right)\sin(\omega_d(t-\tau))d\tau \\ -\int_{t_4}^{t_5} \frac{A_{peak}}{2}\left(1-\cos\frac{\pi}{T_1}(\tau-t_4)\right)\sin(\omega_d(t-\tau))d\tau - \int_{t_5}^{t} A_{peak}\sin(\omega_d(t-\tau))d\tau \end{array}\right] \\ &= \frac{A_{peak}}{\omega_d{}^2}\left[1-\frac{\pi^2}{\pi^2-(\omega_d T_1)^2}\cos\left(\frac{\omega_d T_1}{2}\right)\left[\cos\left(\omega_d\left((t-t_4)-\frac{T_1}{2}\right)\right)+2\sin\left(\frac{\omega_d(T_1+T_2)}{2}\right)\sin\left(\omega_d\left((t-t_0)-T_1-\frac{T_2}{2}\right)\right)\right]\right] \end{aligned}, \quad (26)$$

and the dynamic response during the constant velocity segment $[t_3,\ t_4]$ can be derived as follows:

$$\begin{aligned} y(t|t_3 \leq t < t_4) &= -\frac{1}{\omega_d}\left[\begin{array}{l} \int_{t_0}^{t_1} \frac{A_{peak}}{2}\left(1-\cos\frac{\pi}{T_1}(\tau-t_0)\right)\sin(\omega_d(t-\tau))d\tau + \int_{t_1}^{t_2} A_{peak}\sin(\omega_d(t-\tau))d\tau \\ +\int_{t_2}^{t_3} \frac{A_{peak}}{2}\left(1+\cos\frac{\pi}{T_1}(\tau-t_2)\right)\sin(\omega_d(t-\tau))d\tau \end{array}\right] \\ &= -\frac{2A_{peak}}{\omega_d{}^2}\frac{\pi^2}{\pi^2-(\omega_d T_1)^2}\cos\left(\frac{\omega_d T_1}{2}\right)\sin\left(\frac{\omega_d(T_1+T_2)}{2}\right)\sin\left(\omega_d\left((t-t_0)-T_1-\frac{T_2}{2}\right)\right) \end{aligned}. \quad (27)$$

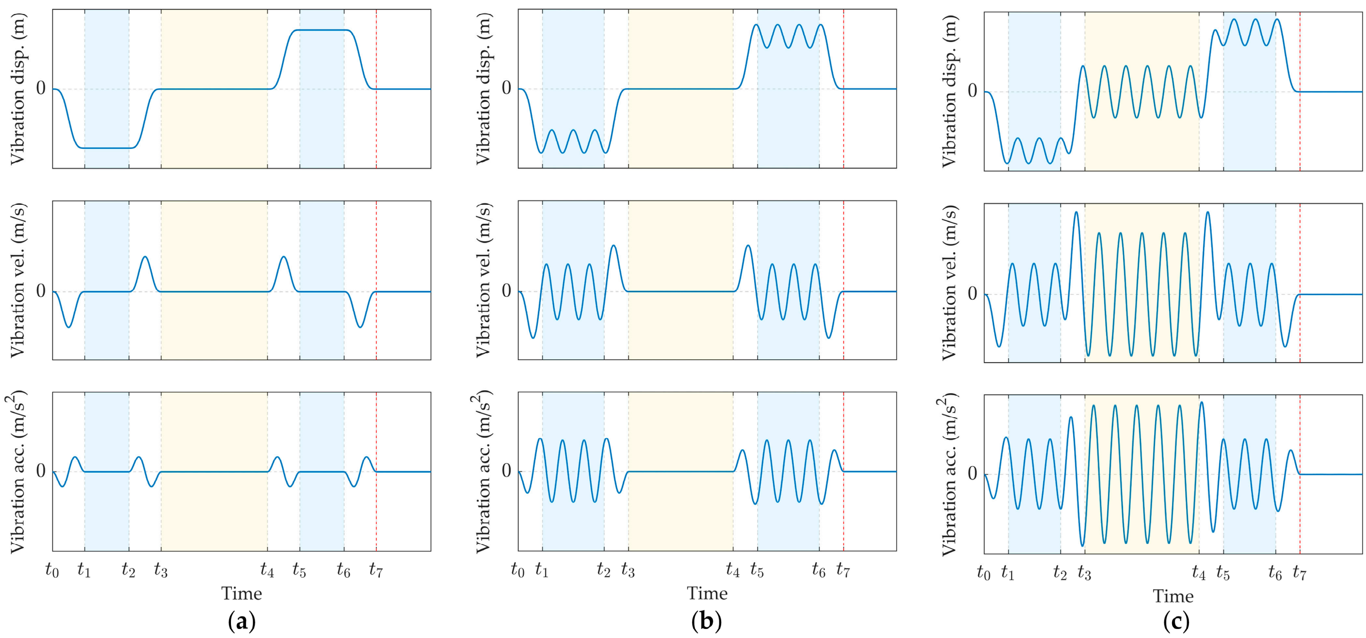

Figure 5. Vibration responses of sinusoidal jerk profile optimized under different suppression conditions: (**a**) only condition C1 is satisfied; (**b**) only condition C2 is satisfied; (**c**) only condition C3 is satisfied.

Substituting (22) into (25)–(27) yields the following:

$$y(t|t_1 \leq t < t_2) = -\frac{A_{peak}}{\omega_d{}^2},\ y(t|t_5 \leq t < t_6) = \frac{A_{peak}}{\omega_d{}^2},\ y(t|t_3 \leq t < t_4) = 0. \quad (28)$$

Equation (28) implies that satisfying C1 leads to zero vibrations during the constant acceleration segments and constant velocity segment (see Figure 5a). The physical meaning of this condition is that the vibrations induced in the sinusoidal jerk segments are offset at the end of these segments ($t = t_1, t_3, t_5, t_7$). Likewise, it can be observed that if C2 is satisfied, then the vibrations induced in the positive sinusoidal jerk segment $[t_0,\ t_1]$ and the negative sinusoidal jerk segment $[t_2,\ t_3]$ cancel each other out at the end of the acceleration phase ($t = t_3$), ensuring no vibrations during the constant velocity segment (see Figure 5b). In contrast, these properties are not present for C3. The vibration induced in the acceleration phase counteracts that in the deceleration phase, and only the residual vibration after the motion stops is suppressed (see Figure 5c). Therefore, when a smooth transfer is required in the movement, condition C1 should be preferentially selected for parameter tuning. Unless otherwise specified, the scheme will choose the one that produces a shorter moving time.

Note that these conditions depend on the system parameter ω_d and are thus influenced by the accuracy of the parameter estimation. In cases in which parameter estimation errors occur or vibration modes vary during motion, it is expected that the motion profile will remain robust against parameter variations. One solution is to prolong the motion time length, as it reduces both the frequency range and amplitudes of the acceleration profile. However, this would lead to much slower movement, which is undesirable in production. Alternatively, the robustness against system parameter uncertainties can be improved when the profile parameters satisfy multiple conditions from C1 to C3, which can be evaluated by taking partial derivatives of the vibration amplitude with respect to the estimated natural frequency. Particularly, if two of the vibration suppression conditions are satisfied for a given value of ω_d, the following holds:

$$y_{res}(\omega_d) = \frac{\partial y_{res}(\omega_d)}{\partial \omega_d} = 0. \tag{29}$$

Thus, for a small estimation error ($\Delta\omega_d$), we have the following:

$$y_{res}(\omega_d + \Delta\omega_d) \cong y_{res}(\omega_d) + \frac{\partial y_{res}(\omega_d)}{\partial \omega_d} \cdot \Delta\omega_d \cong 0. \tag{30}$$

Equation (30) reveals that the residual-vibration amplitude is not only zero at ω_d but is also approximately zero near ω_d, which implies that the vibration is robustly mitigated even with a parameter estimation error to some extent. Similarly, if all three vibration suppression conditions are satisfied, then the insensitivity performance is further enhanced, as the following holds:

$$\frac{\partial^2 y_{res}(\omega_d)}{\partial^2 \omega_d} = 0. \tag{31}$$

In fact, the first and second derivatives with respect to the nominal natural frequency represent, respectively, the gradient and curvature of the vibration amplitude evolution curve versus the estimated frequency. If both of these derivatives are equal to zero, then the vibrations remain limited within a broader frequency band, enabling the motion profile to effectively handle the system uncertainties typically encountered in practice. In what follows, the motion profiles that satisfy one, two, and three conditions are referred to as onefold, twofold, and threefold vibration mitigation, respectively. The robustness degrees for the three cases are defined as r = 1, 2, and 3, respectively. This degree can be specified by the user according to actual demands in applications.

From a spectral point of view, tuning the profile parameters essentially removes the frequency content of the input motion profile that is related to the resonances. When the vibration suppression conditions are met, the frequency spectrum of the reference acceleration profile exhibits zero magnitude at the resonant frequency, aligning with the system's pole. As a matter of fact, a mechanical system functions as a filter that amplifies or diminishes the magnitudes of different harmonics based on its frequency response. The frequency contents near the resonances in the input are significantly amplified. To more clearly illustrate this point, we consider the expression of the acceleration profile $a(t)$ in (5) in the Laplace domain:

$$A(s) = \frac{A_{peak}}{2}\left(\frac{\pi}{t_1}\right)^2 \frac{\left(1+e^{-st_1}\right)\left(1-e^{-st_2}\right)\left(1-e^{-st_4}\right)}{\left[s^2+\left(\frac{\pi}{t_1}\right)^2\right]s}. \quad (32)$$

Thus, the frequency spectrum of the acceleration profile can be deduced as follows:

$$|A(j\omega)| = \left|\frac{A_{peak}}{2}\left(\frac{\pi}{t_1}\right)^2 \frac{\left(1+e^{-j\omega t_1}\right)\left(1-e^{-j\omega t_2}\right)\left(1-e^{-j\omega t_4}\right)}{\left[-\omega^2+\left(\frac{\pi}{t_1}\right)^2\right]j\omega}\right| = \frac{\left|4D\cos\left(\frac{\omega t_1}{2}\right)\sin\left(\frac{\omega t_2}{2}\right)\sin\left(\frac{\omega t_4}{2}\right)\right|}{\left|\left(1-\left(\frac{\omega t_1}{\pi}\right)^2\right)\omega t_2 t_4\right|}. \quad (33)$$

Note that if any one of the conditions C1, C2, or C3 is satisfied, $|A(j\omega)|$ is equal to zero at $\omega = \omega_d$. Figure 6 gives an example of the acceleration spectra before and after parameter optimization. It can be observed that the contributions of the proposed sinusoidal jerk profile to vibration reduction are twofold: On the one hand, the smoothness of the profile induces a low-pass filtering effect, causing high-frequency components to attenuate rapidly. On the other hand, the optimization of the profile parameters further eliminates frequency contents in the resonant mode that can excite vibrations. As a result, the resonant mode can be effectively mitigated, successfully preventing the excitation of undesirable vibrations.

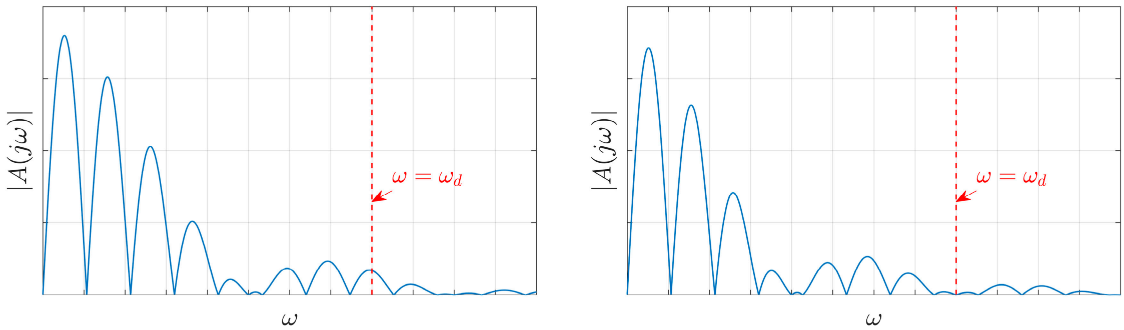

(**a**) Before optimization (**b**) After optimization

Figure 6. Frequency spectra of acceleration profiles.

3.3. Optimization Process for Vibration Suppression

From condition C1 to C3, the solutions for vibration cancellation are clearly infinite in number, as the values of k_1, k_2, and k_3 can take any positive integer. Furthermore, the actuator limits represented by the $V_{\max}$, $A_{\max}$, and $J_{\max}$ should be strictly adhered to for practical feasibility. To generate fast and smooth movements with low vibrations, it is crucial to find the optimal values of T_1, T_2, and T_3 that minimize the motion duration under the actuator limits while satisfying the design constraints of vibration suppression and robustness.

Algorithm 1 provides the parameter optimization procedure for the time–frequency-optimal motion profile. First, the parameters for a minimum-time motion profile with actuator limits are obtained using the formulas described in Section 3.1. Subsequently, these parameters are adjusted to accommodate the vibration characteristics. The number of vibration suppression conditions to be satisfied depends on the desired degree of robustness (r). It is worth noting that the selection of the vibration suppression conditions also impacts the motion duration. In essence, the parameters tuned in these conditions are t_1, t_2, and t_4, and the total motion duration can be expressed as $T_f = t_1 + t_2 + t_4$. Given that the original profile is time-optimal under physical limits, the parameters after modulation, in accordance with the selected conditions, should not be smaller than their original values in order to maintain respect for the physical limits. Tuning different parameters would result in varying time prolongations. Therefore, when selecting the vibration suppression conditions, the objective should be to minimize this prolongation. In addition, for the realization of the motion profile, $t_1 > 0$, $t_2 \geq t_1$ and $t_4 \geq t_1 + t_2$ must be fulfilled based on the pre-conditions $T_1 > 0$, $T_2 \geq 0$, $T_3 \geq 0$. Clearly, if r is set to 1 or 2, then there are three possible choice options: if r = 1, then we can choose C1, C2, or C3; if r = 2, then we can choose (C1, C2), (C1, C3), or (C2, C3); if r = 3, then only one choice (C1, C2, C3) is available. We use a vector (**C**) to represent the selection made, where the conditions that are selected are marked as 1 and the conditions that are not selected are marked as 0. For instance, if only C1 is selected to be satisfied, then **C** = [1 0 0]. The set of possible options is denoted as S.

Algorithm 1: Optimization of profile parameters

Input: moving distance D, actuator limits $V_{\max}$, $A_{\max}$, $J_{\max}$, vibration period T_d, robustness degree r
Output: optimal profile parameters $\hat{T}_1$, $\hat{T}_2$, $\hat{T}_3$, $\hat{J}_{peak}$

Start
Compute the minimum time solution according to Table 1
if r = 1
    S = {[1 0 0], [0 1 0], [0 0 1]}; l = 3
else if r = 2
    S = {[1 1 0], [1, 0, 1], [0, 1, 1]}; l = 3
else
    S = {[1 1 1]}; l = 1
end if
for i = 1 to l **do**
    C = S{i}
    Modulate $\hat{t}_1$, $\hat{t}_2$ and $\hat{t}_4$ using Equations (34)–(36)
    Compute the total execution time $T_f = \hat{t}_1 + \hat{t}_2 + \hat{t}_4$
end for
find **C** = S{i} $\in$ S that minimizes T_f
Compute the optimal parameters $\hat{T}_1$, $\hat{T}_2$, $\hat{T}_3$, $\hat{J}_{peak}$
end

In order to draw a distinction from the initial minimum-time solution, the caret symbol (ˆ) is added to indicate the variables associated with the final time–frequency-optimal motion profile. Thus, for a specific **C**, the parameters are modulated as follows:

$$\hat{t}_1 = \begin{cases} t_1, & \mathbf{C}(1) = 0 \\ \left(\max\left\{\mathrm{ceil}\left(\frac{t_1 - T_d/2}{T_d}\right),\, 1\right\} + \frac{1}{2}\right)T_d, & \mathbf{C}(1) = 1 \end{cases}, \tag{34}$$

$$\hat{t}_2 = \begin{cases} \max\{\hat{t}_1, t_2\}, & \mathbf{C}(2) = 0 \\ \mathrm{ceil}\left(\frac{\max\{\hat{t}_1, t_2\}}{T_d}\right)T_d, & \mathbf{C}(2) = 1 \end{cases}, \tag{35}$$

$$\hat{t}_4 = \begin{cases} \max\{\hat{t}_1 + \hat{t}_2, t_4\}, & \mathbf{C}(3) = 0 \\ \mathrm{ceil}\left(\frac{\max\{\hat{t}_1 + \hat{t}_2, t_4\}}{T_d}\right)T_d, & \mathbf{C}(3) = 1 \end{cases}, \tag{36}$$

where ceil($\cdot$) rounds a number up to the nearest integer greater than or equal to the given argument, and max($\cdot$) returns the largest element among a collection of input values. This modulation ensures both the suppression of the residual vibration and the minimization of the introduced time delay without violating any constraints. The conformity to the actuator limits is always ensured, as the values of the parameters $\hat{t}_1$, $\hat{t}_2$, and $\hat{t}_4$ after modulation are not smaller than their initial values computed in Table 1. This is evident from the relationship between these parameters and the peak kinematic values:

$$\hat{V}_{peak} = \frac{D}{\hat{t}_4},\ \hat{A}_{peak} = \frac{D}{\hat{t}_2\hat{t}_4},\ \hat{J}_{peak} = \frac{\pi D}{2\hat{t}_1\hat{t}_2\hat{t}_4}. \tag{37}$$

All possible options in S should be computed to find the optimal selection **C** that minimizes the total motion duration. Finally, once the optimal values of $\hat{t}_1$, $\hat{t}_2$, and $\hat{t}_4$ are obtained, the time parameters $\hat{T}_1$, $\hat{T}_2$, and $\hat{T}_3$ are computed via $\hat{T}_1 = \hat{t}_1$, $\hat{T}_2 = \hat{t}_2 - \hat{t}_1$, and $\hat{T}_3 = \hat{t}_4 - \hat{t}_2 - \hat{t}_1$, respectively.

So far, a closed-form solution for the optimal sinusoidal jerk profile has been derived. The optimized motion profile minimizes the execution time to achieve fast movement while considering the actuator capacities, vibration cancelation, and robustness constraints.

The final implementation procedure for practical applications of the developed methodology is as follows: (1) user: definition of the desired displacement and physical limits according to the machine specifications and task requirements; (2) host computer: computation of the optimal profile parameters through computing tools such as Matlab or Python and the generation of the motion profile; (3) machine controller: reception of the motion profile data from the host computer and their transfer to driving commands; (4) driver: execution of the motion profile according to the driving commands sent by the controller.

4. Numerical Results

In this section, the effectiveness of the proposed profile design scheme is validated via a series of simulation studies. The sinusoidal jerk motion profile is compared to other classic motion laws (i.e., the trapezoidal velocity profile and S-curve profiles) from kinematic and dynamic points of view, which are detailed in Sections 4.1 and 4.2, respectively.

4.1. Kinematic Comparative Study

To verify the feasibility and versatility of the method, the study was conducted with various constraint conditions, as listed in Table 2. In addition, it was assumed that the natural frequency of the system is 8 Hz, with a damping ratio of 0.01 (T_d = 0.125 s). Both the minimum-time and time–frequency-optimal sinusoidal jerk profiles adapted to the vibration characteristics were generated. Note that for the latter, the robustness degree specified by the user affects the resulting profile. In the first study, this degree was set to r = 1. The parameters of the minimum-time sinusoidal jerk profiles and the optimized sinusoidal jerk profiles were solved according to the algorithms in Sections 3.1 and 3.3, respectively. These optimization algorithms were implemented in the Matlab language, and the conditions listed in Table 2 were used as the input arguments. Tables 3 and 4 contain the values of the obtained profile parameters, along with the total durations of the resulting profiles. Then, the corresponding displacement, velocity, acceleration, and jerk profiles were obtained by applying the formulations in Section 2.2.

The results under different constraints are illustrated in Figures 7–10. It is recognized that the yielded motion profiles for all the test cases successfully arrive at the desired positions while strictly complying with the actuator limits, demonstrating the high reliability of the method. Moreover, within each segment of the minimum-time sinusoidal jerk profiles, the peak value of a derivative equals the corresponding bound. As a consequence, the duration of this motion profile cannot be further shortened without violating any of the imposed constraints. In contrast, the peak kinematic values of the time–frequency-optimal profiles are slightly smaller than their bound values due to the fine tuning of the time parameter for vibration mitigation.

Table 2. Constraint conditions for computation of motion profiles.

Case	D (m)	V_{max} (m/s)	A_{max} (m/s^2)	J_{max} (m/s^3)
1	0.75	0.8	4	60
2	0.32	1	1.5	40
3	0.32	0.25	2.4	30
4	0.08	0.5	3	30

Table 3. Parameters of minimum-time sinusoidal motion profiles.

Case	T_1 (s)	T_2 (s)	T_3 (s)	T_f (s)
1	0.1047	0.0953	0.6328	1.2422
2	0.0589	0.3745	0	0.9845
3	0.1144	0	1.0512	1.5088
4	0.1279	0	0	0.5118

Table 4. Parameters of optimized sinusoidal motion profiles ($r = 1$).

Case	Selection	T_1 (s)	T_2 (s)	T_3 (s)	T_f (s)
1	C2	0.1047	0.1453	0.5828	1.2922
2	C3	0.0589	0.3745	0.0078	0.9923
3	C2	0.1144	0.0106	1.0406	1.5194
4	C3	0.1279	0	0.1191	0.6309

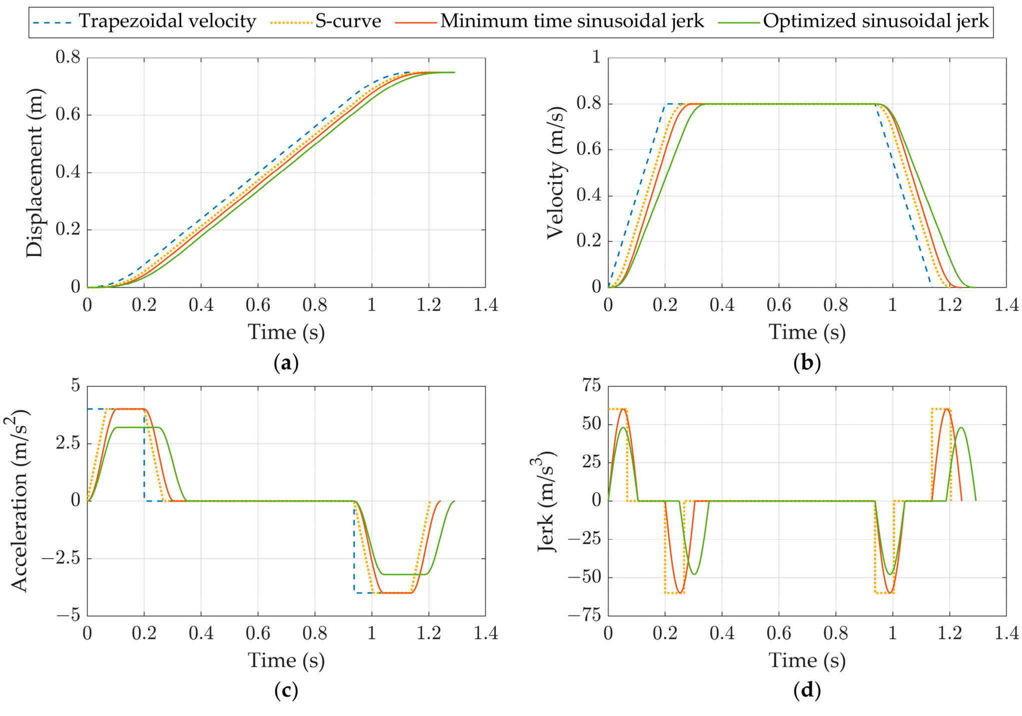

Figure 7. Motion profiles resulting from different techniques in Case 1: (**a**) displacement; (**b**) velocity; (**c**) acceleration; (**d**) jerk.

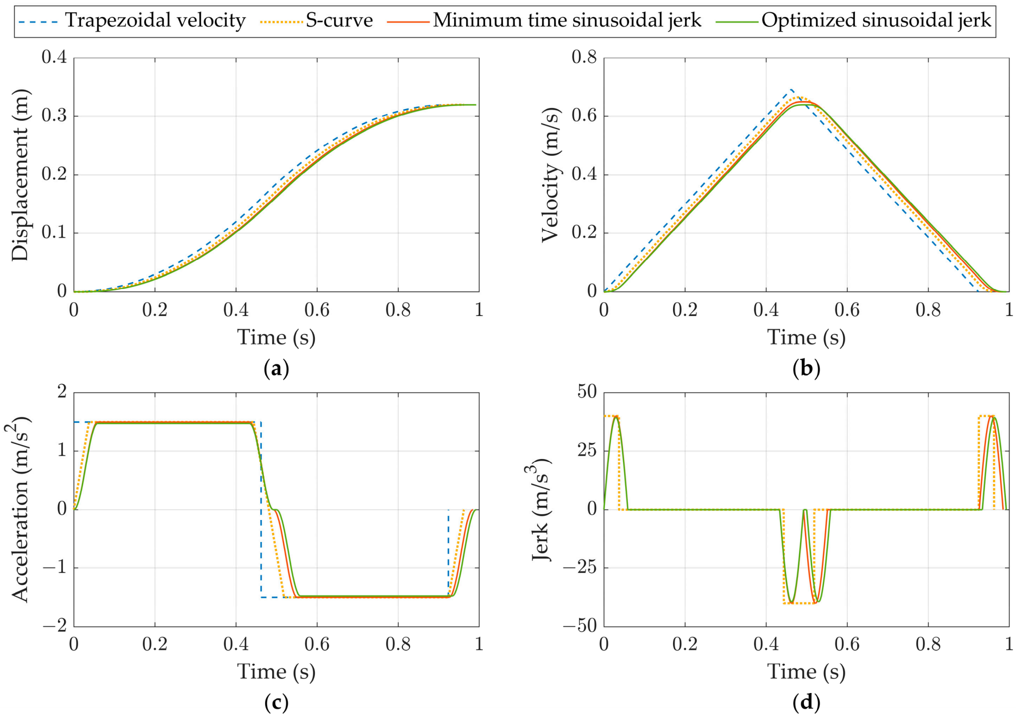

Figure 8. Motion profiles resulting from different techniques in Case 2: (**a**) displacement; (**b**) velocity; (**c**) acceleration; (**d**) jerk.

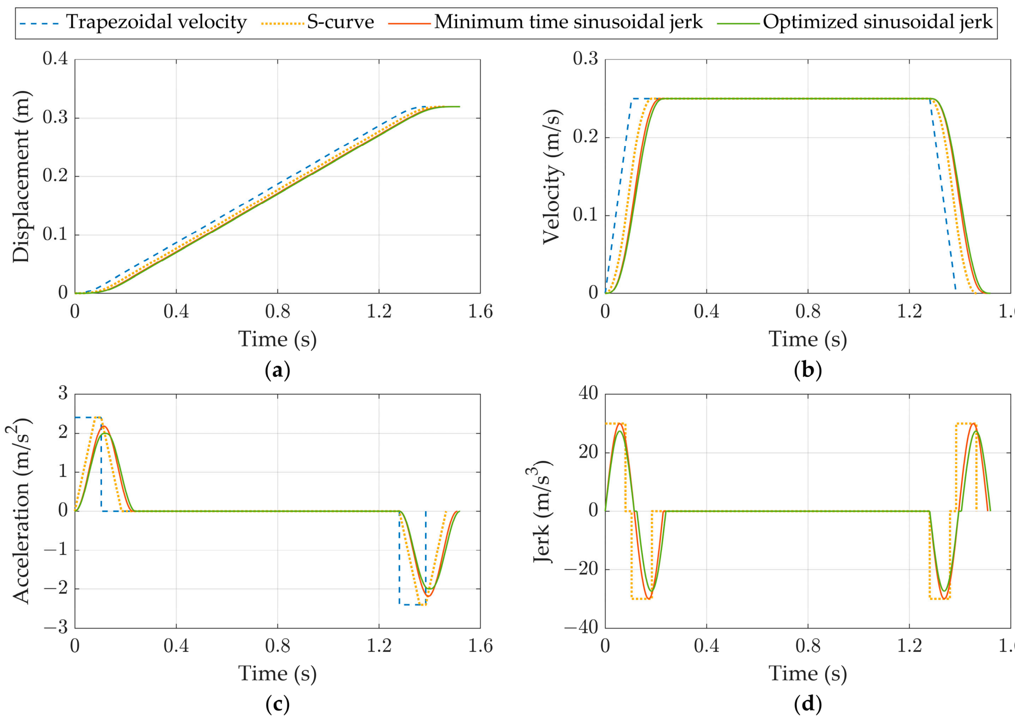

Figure 9. Motion profiles resulting from different techniques in Case 3: (**a**) displacement; (**b**) velocity; (**c**) acceleration; (**d**) jerk.

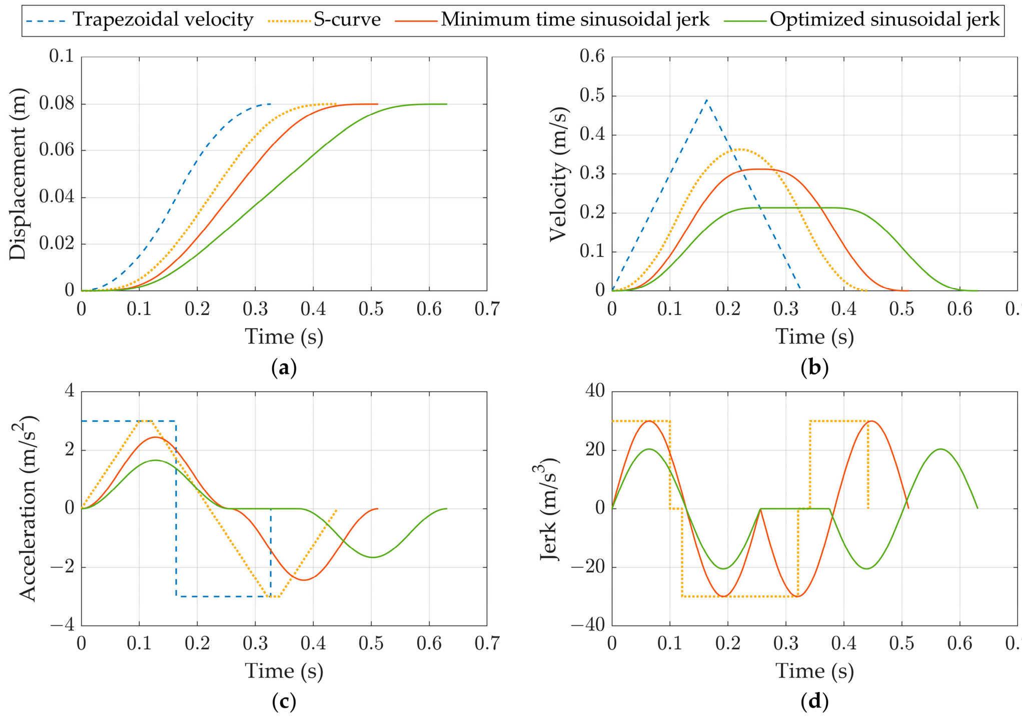

Figure 10. Motion profiles resulting from different techniques in Case 4: (**a**) displacement; (**b**) velocity; (**c**) acceleration; (**d**) jerk.

For Case 1 shown in Figure 7, all the kinematic limit values are reached in the minimum-time sinusoidal jerk profile, which is a standard seven-segment profile. Because the r is set to 1, we can choose one condition from C1, C2, and C3. By applying the algorithm from Section 3.3, the motion durations (T_f) corresponding to different conditions are computed. Specifically, if C1 is selected, then T_f = 1.3250 s; if C2 is selected, then T_f = 1.2922 s; and if C3 is selected, then T_f = 1.3048 s. Therefore, to minimize the motion duration, condition C2 is finally selected for parameter tuning to achieve the time–frequency-optimal sinusoidal jerk profile. The optimal solution is T_1 = 0.1047 s, T_2 = 0.1453 s, T_3 = 0.5828 s, and $J_{\max}$ = 0.1047 s, such that T_1 + T_2 is equal to two vibration periods (i.e., $t_2 = 2T_d$). The total duration of the optimal profile (1.2922 s) is only 0.05 s longer than the original one (1.2422 s). For Case 2 shown in Figure 8, the maximum allowable velocity is not reached in the minimum-time profile because of the relatively short moving distance, and, accordingly, the constant velocity segment vanishes. In this case, the optimization procedure modifies T_3 to satisfy condition C3, resulting in an optimal profile with seven segments. Similarly, in Case 3 depicted in Figure 9, the maximum allowable acceleration is not attained for the minimum profile due to the velocity limit, and thus the constant acceleration segment is absent. The application of the proposed optimization procedure on the time parameters leads to the optimal profile that satisfies condition C2. Finally, the minimum-time profile is composed of only sinusoidal jerk segments in the last case, as none of the kinematic bounds are attainable due to the limitation on the moving distance. With condition C3 selected, the original motion profile becomes a five-segment profile after tuning T_3, as illustrated in Figure 10.

The trapezoidal velocity and S-curve motion profiles generated with the same constraints are also shown in Figures 7–10 for comparison. The trapezoidal velocity profile exhibits infinite jerk due to acceleration discontinuities, while the S-curve profile effectively limits jerk but still experiences jerk discontinuities at segment switching times. Compared to the trapezoidal velocity and S-curve profiles, the sinusoidal jerk profile features better smoothness, ensuring continuous velocity, acceleration, and jerk. An associated trade-off with this smoothness improvement is a slight increase in the motion duration. However, this increase in the motion duration is adequately compensated for by the shortened settling time, which will be clarified in the next subsection.

4.2. Comparative Dynamic Study

To assess the influence of the motion laws on residual vibrations, the dynamic model of a flexible-motion system (Figure 4) was taken into account for comparative analysis. This simplified model can effectively represent a wide range of industrial equipment, such as transfer robots, inspection machines, and cranes. The motion profiles obtained in the last subsection were utilized as the reference input to the system in order to evaluate the response of the mass following the previous settlings: ω_n = 50.27 rad/s and ζ = 0.01. The simulation was performed in the Matlab/Simulink environment, and Figure 11 depicts the model of the dynamic response of the mass. The time step was set to 0.5 ms.

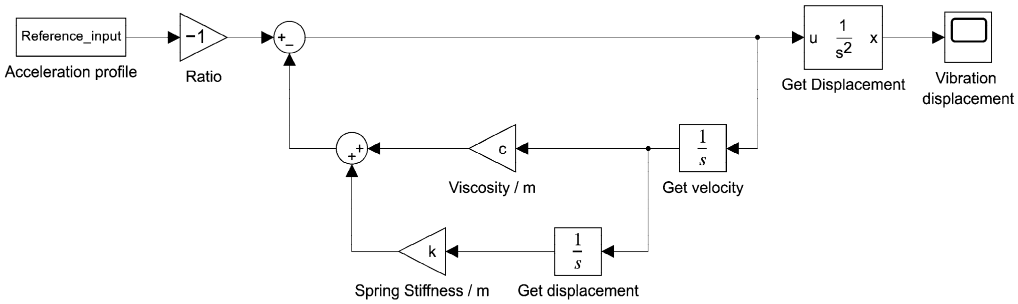

Figure 11. Simulation model for motion-induced vibration.

Figures 12–15 depict the vibration responses with different profiles for Cases 1–4. The vertical dashed lines marked in corresponding colors represent the motion completion times for the profiles. The same applies to the subsequent figures. Table 5 reports the comparison results in terms of the peak-to-peak value of the residual vibration and settling time, with the values in bold indicating the best results achieved among these profiles. The settling time is defined as the time at which the induced vibration decays and remains within a specified error band (±0.2 mm). It can be observed that the vibration level decreased remarkably with an increase in the continuity of the motion profiles, albeit at the expense of a slight prolongation of the duration.

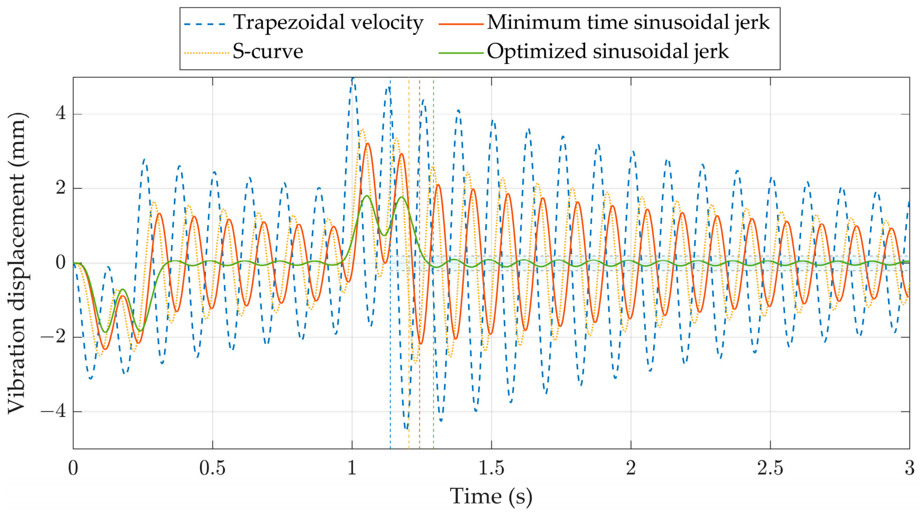

Figure 12. Comparison of vibration responses induced by different motion profiles in Case 1.

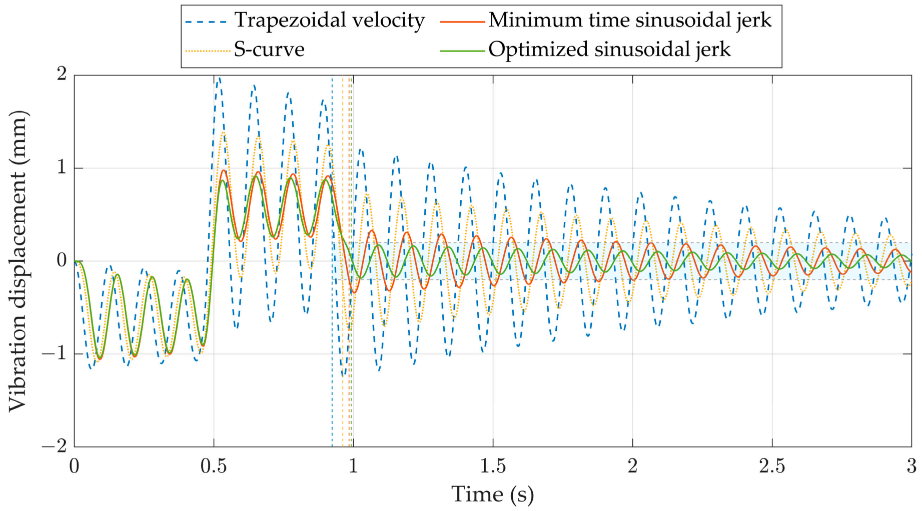

Figure 13. Comparison of vibration responses induced by different motion profiles in Case 2.

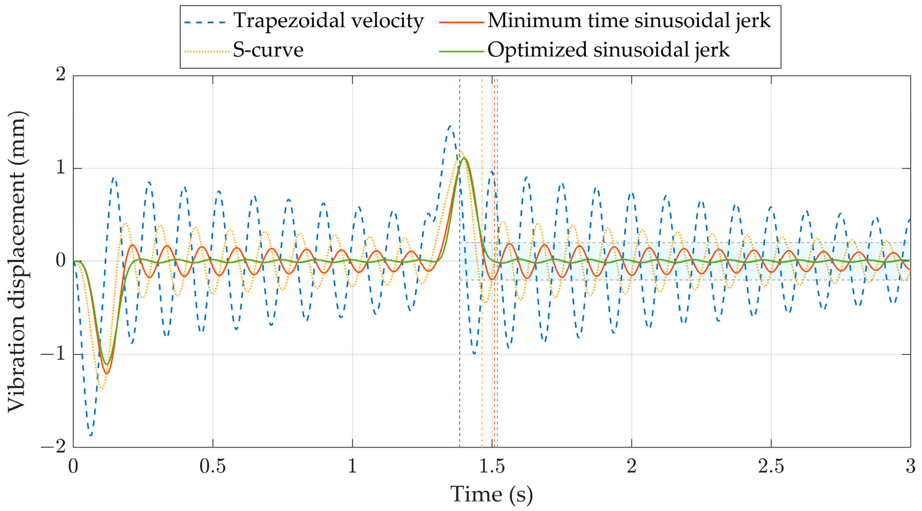

Figure 14. Comparison of vibration responses induced by different motion profiles in Case 3.

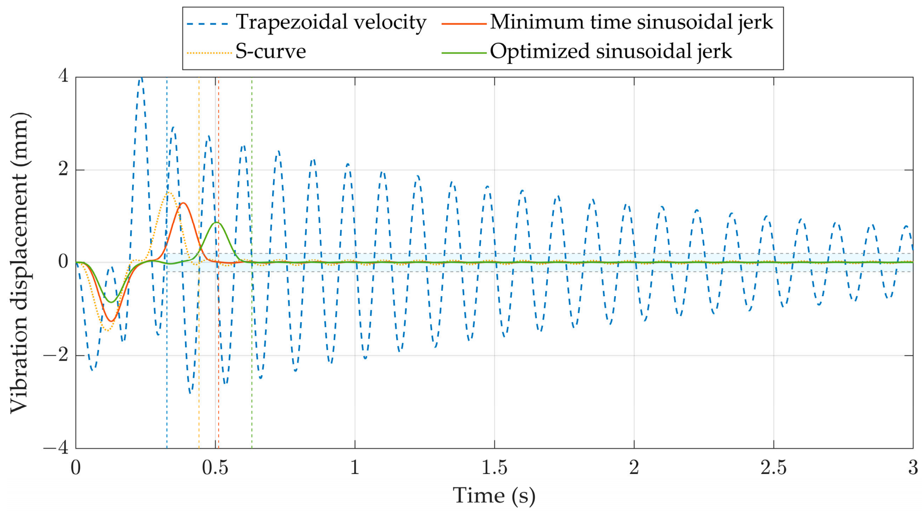

Figure 15. Comparison of vibration responses induced by different motion profiles in Case 4.

Table 5. Numerical comparison results of residual vibrations and settling times induced by different motion profiles.

Case		Motion Profile			
		Trapezoidal Velocity	S-Curve	Minimum-Time Sinusoidal Jerk	Optimized Sinusoidal Jerk
1	Residual vibration (mm)	8.913 (ref)	5.293 (−40.6%)	4.306 (−51.7%)	**0.224** * (−97.5%)
	Settling time (s)	7.385 (ref)	6.357 (−13.9%)	5.999 (−18.8%)	**1.292** * (−82.5%)
2	Residual vibration (mm)	2.479 (ref)	1.473 (−40.6%)	0.672 (−72.9%)	**0.359** * (−85.5%)
	Settling time (s)	4.594 (ref)	3.554 (−22.6%)	2.067 (−55%)	**0.992** * (−78.4%)
3	Residual vibration (mm)	1.960 (ref)	0.880 (−55.1%)	0.373 (−80.9%)	**0.041** * (−97.9%)
	Settling time (s)	4.626 (ref)	3.044 (−34.2%)	**1.509** * (−67.4%)	1.520 (−67.2%)
4	Residual vibration (mm)	5.743 (ref)	0.143 (−97.5%)	0.027 (−99.5%)	**0.010** * (−99.8%)
	Settling time (s)	5.665 (ref)	**0.442** * (−92.2%)	0.512 (−91%)	0.631 (−88.9%)

* The values in bold indicate the best results achieved among the tested profiles.

As expected, the trapezoidal profile, characterized by acceleration discontinuities, induced the most severe residual vibrations in all the cases, whereas the proposed optimized sinusoidal jerk profile exhibited the best performance in vibration mitigation. In addition, the minimum-time sinusoidal jerk outperformed the trapezoidal velocity and S-curve profiles, which is consistent with observations in previous literature. Specifically, the residual-vibration level generated by the optimized sinusoidal jerk profile decreased by an average of 95.2% relative to the trapezoidal velocity profile, and by 89.9% relative to the S-curve profile. Meanwhile, the settling time, which serves as a reliable productivity metric, was significantly shortened when using the optimized profile for Cases 1 and 2. In all the test cases, the settling times were identical to the motion durations (T_f), as the vibration magnitudes fell below the specified error after reaching the target positions. Hence, in terms of the settling time, the optimized sinusoidal jerk profile achieves the most efficient movement, despite having a slightly longer duration than the other profiles.

To further evaluate the robustness of the method, we performed experiments considering a 10% estimation error in the natural frequency (the actual natural frequency varies from 8 Hz to 7.2 Hz). As mentioned earlier, setting a higher robustness degree (r) enhances the insensitivity of the generated sinusoidal jerk profile to parameter uncertainties. Tables 6 and 7 aggregate the computed parameters for the optimized profiles with the r set to 2 and 3, respectively. Note that these profiles were tuned according to the nominal natural frequency. The vibration responses for the optimized sinusoidal jerk profiles with different robustness degrees in the absence and presence of a modeling error are plotted in Figures 16–19, and the comparison results are summarized in Table 8.

Table 6. Parameters of optimized sinusoidal motion profiles (r = 2).

Case	Selection	T_1 (s)	T_2 (s)	T_3 (s)	T_f (s)
1	C2, C3	0.1047	0.1453	0.6453	1.3548
2	C2, C3	0.0589	0.4411	0.0661	1.1840
3	C2, C3	0.1144	0.0106	1.1357	1.6145
4	C1, C3	0.1875	0	0	0.7500

Table 7. Parameters of optimized sinusoidal motion profiles (r = 3).

Case	Selection	T_1 (s)	T_2 (s)	T_3 (s)	T_f (s)
1	C1, C2, C3	0.1875	0.0625	0.5625	1.4376
2	C1, C2, C3	0.1875	0.3125	0.0625	1.4376
3	C1, C2, C3	0.1875	0.0625	0.9375	1.8126
4	C1, C2, C3	0.1875	0.0625	0.0625	0.9375

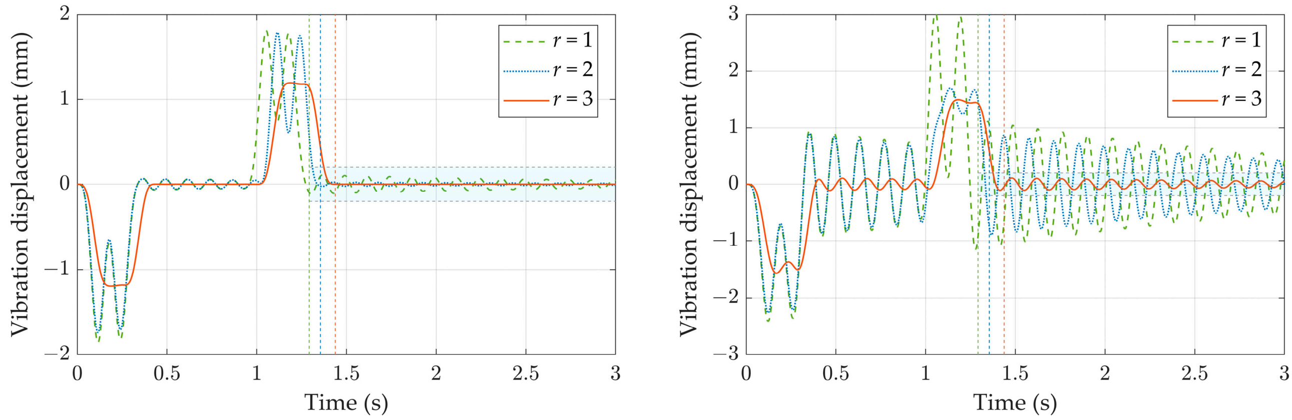

(**a**) Without modeling error (**b**) With modeling error

Figure 16. Vibration responses for optimized sinusoidal jerk profiles with different robustness degrees in Case 1.

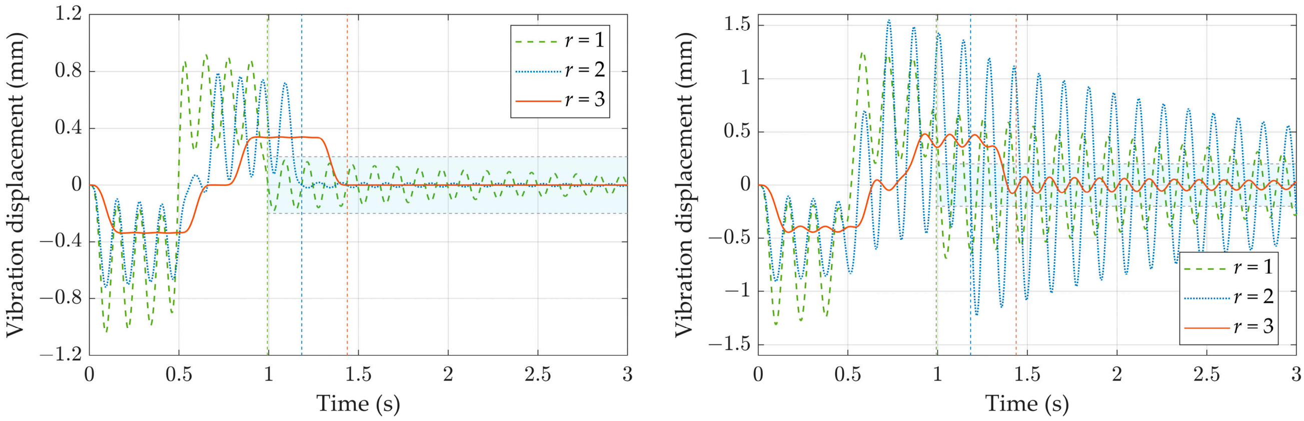

(**a**) Without modeling error (**b**) With modeling error

Figure 17. Vibration responses for optimized sinusoidal jerk profiles with different robustness degrees in Case 2.

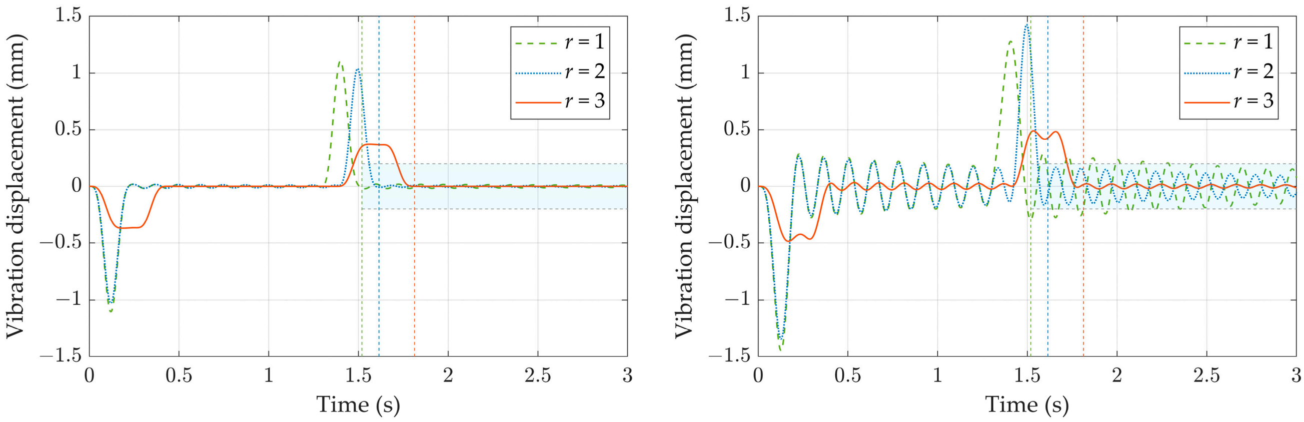

(**a**) Without modeling error (**b**) With modeling error

Figure 18. Vibration responses for optimized sinusoidal jerk profiles with different robustness degrees in Case 3.

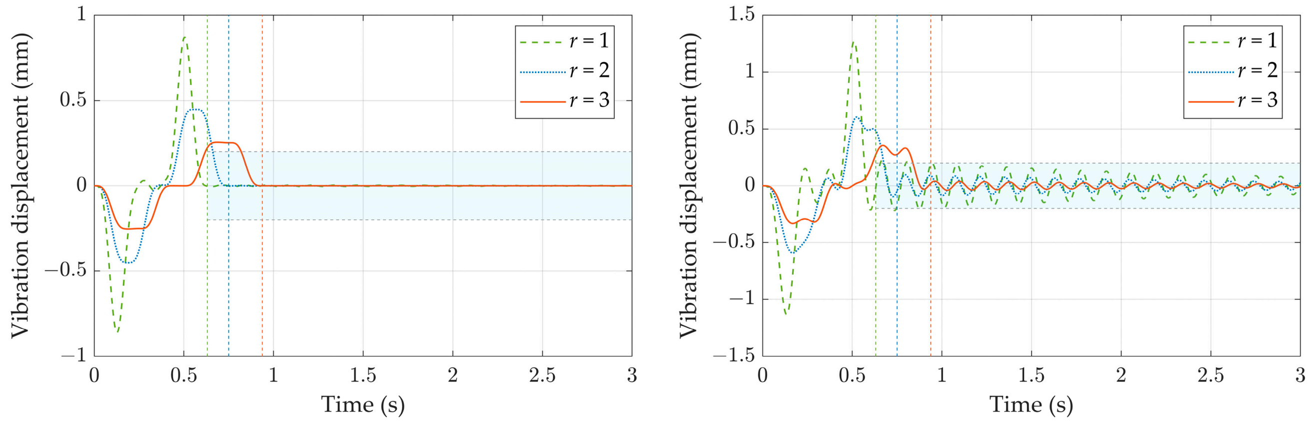

(**a**) Without modeling error (**b**) With modeling error

Figure 19. Vibration responses for optimized sinusoidal jerk profiles with different robustness degrees in Case 4.

Table 8. Comparative results of optimized sinusoidal jerk profiles with different robustness degrees with/without modeling errors.

Case		***r* = 1**		***r* = 2**		***r* = 3**	
		w/o Modeling Error	**w/ Modeling Error**	**w/o Modeling Error**	**w/ Modeling Error**	**w/o Modeling Error**	**w/ Modeling Error**
1	Residual vibration (mm) Settling time (s)	0.224 **1.292** * (ref)	2.201 5.102 (+295%)	0.051 1.355 (ref)	1.768 4.637 (+242%)	**0.001** * 1.438 (ref)	**0.221** * **1.438** * (+0%)
2	Residual vibration (mm) Settling time (s)	0.359 **0.992** * (ref)	1.362 3.760 (+279%)	0.037 1.184 (ref)	2.418 5.182 (+338%)	**0** * 1.438 (ref)	**0.156** * **1.438** * (+0%)
3	Residual vibration (mm) Settling time (s)	0.041 **1.520** * (ref)	0.564 2.356 (+55%)	0.018 1.615 (ref)	0.332 **1.615** * (+0%)	**0** * 1.813 (ref)	**0.045** * 1.813 (+0%)
4	Residual vibration (mm) Settling time (s)	0.010 **0.631** * (ref)	0.445 0.881 (+39.6%)	0.002 0.750 (ref)	0.190 **0.750** * (+0%)	**0** * 0.938 (ref)	**0.081** * 0.938 (+0%)

* The values in bold indicate the best results achieved among the tested profiles.

As shown in Table 8, under nominal conditions, all the optimized sinusoidal jerk profiles effectively attenuated the residual vibrations. However, when an estimation error was introduced, the residual-vibration levels increased in all the test cases. It is worth noting that the optimized profiles with onefold vibration mitigation produced noticeably larger vibrations as the resonant frequency deviated, resulting in a certain degree of performance degradation. In contrast, the optimized profile with threefold vibration mitigation achieved a superior robustness performance under the frequency perturbation, leading to the smallest increment in the residual vibrations. The profile with twofold vibration mitigation was characterized by an intermediate robustness between the profiles with twofold and twofold vibration mitigation. This difference can also be observed with ease by measuring the setting times. Table 8 reports the percentage increments in the settling time due to the modeling error for each motion profile. On average, the increments in the settling time for the profiles with onefold and twofold vibration mitigation are 167% and 145%, respectively, while the settling times for the profiles with threefold vibration mitigation remain the same as the moving time (T_f).

To better quantify the influence of the parameter perturbations on the results, the magnitude evolution curves of the residual-vibration envelope with respect to a $\pm$ 10% variation in the actual natural frequency in the four test cases are plotted in Figure 20. The results confirm the consistency of the sensitivity reduction brought on by the optimized profiles with threefold vibration mitigation. The vibration level remains limited within the allowed tolerance despite minor parameter perturbations, as the harmonic contents are eliminated in a wider neighborhood of the resonant frequency with the increase in the r. Therefore, the motion profile with threefold vibration reduction is preferable in the presence of system modeling errors.

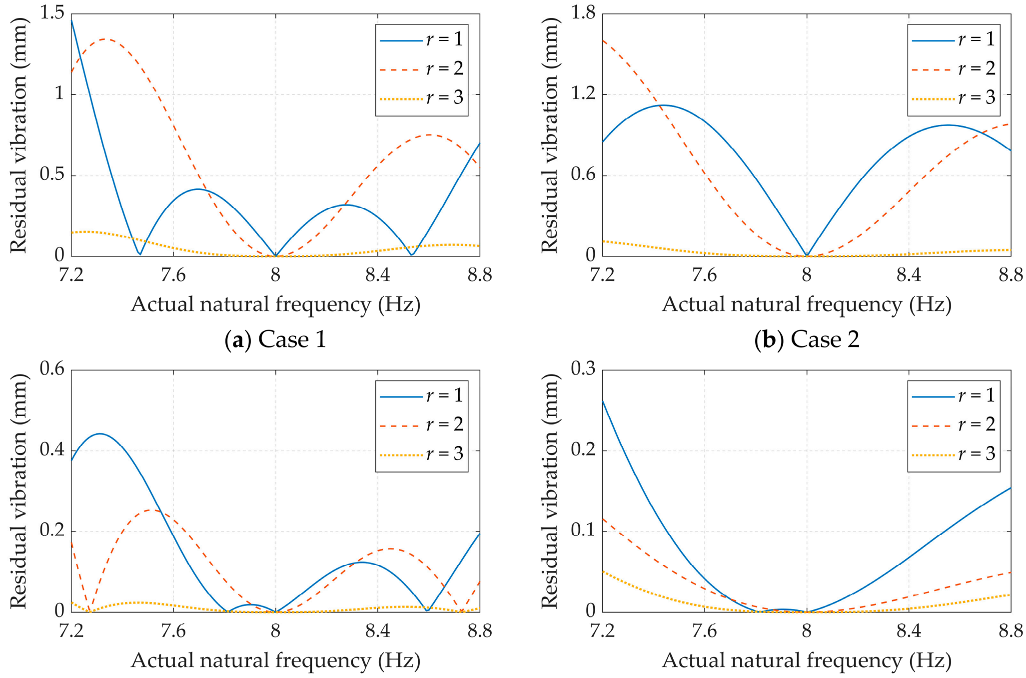

(**a**) Case 1 (**b**) Case 2

(**c**) Case 3 (**d**) Case 4

Figure 20. Magnitude of residual-vibration envelope for ±10% variation in actual natural frequency with optimized sinusoidal jerk profiles.

5. Experimental Results

To further verify the practicality of the proposed method, experiments were conducted on a linear-motion stage manufactured by PARADOX Inc., which is commonly used in production equipment such as bonding machines, transfer robots, inspection instruments, and dispensers. A stainless-steel beam was attached to the base to imitate the flexible behavior of the tool side. During operation, high-speed movements of the stage base can induce vibrations in the beam along the motion direction that need extra standby time to dissipate at the end positions. Minimizing the induced vibrations is crucial for improving the positioning accuracy and efficiency. The motion stage was controlled by a host computer through a motion control board (GHN, Googoltech) connected via the gLink-II bus. The optimization algorithms were programmed and implemented on the host computer, and the resulting motion profiles were subsequently sent to the control board as the reference input to drive the motor. To measure the vibration accelerations at the beam tip, an accelerometer (1B103, DHTEST) was utilized, with a sampling frequency of 5.12 kHz. The experiment platform is depicted in Figure 21.

In the experiment, the motion stage was required to travel a distance of 0.3 m, and the actuator limits were specified as follows: $V_{\max}$ = 0.4 m/s, $A_{\max}$ = 2 m/s^2, and $J_{\max}$ = 20 m/s^3. The beam was characterized by a natural frequency of 8.81 Hz and a damping ratio of 0.008. The desired positioning accuracy at the target point was set to ± 0.2 m/s^2. The proposed optimized sinusoidal jerk profile, as well as other baseline methods in previous studies [16,23], were tested. Figure 22 shows the actual position profiles of the base read from the linear encoder and the velocity profiles deduced from the derivation of the actual positions. It can be seen that the actual profiles of the base are basically consistent with the reference design and accurately reach the desired positions. Figure 23 illustrates the measured vibration accelerations corresponding to different profiles. An additional test was performed to verify the robustness of the profiles by attaching an extra mass at the beam tip, causing its natural frequency to change from 8.81 Hz to 7.55 Hz, which represents a modeling error of 14.3%. Figures 24 and 25 illustrate the measured vibration accelerations with modeling errors corresponding to the baseline profiles and the optimized sinusoidal jerk profile with different robustness degrees. To evaluate the overall energy distribution across the frequency spectrum, the power spectral density (PSD) curves of the vibration signals with each profile are plotted in Figure 26. The quantitative experimental results are summarized in Table 9.

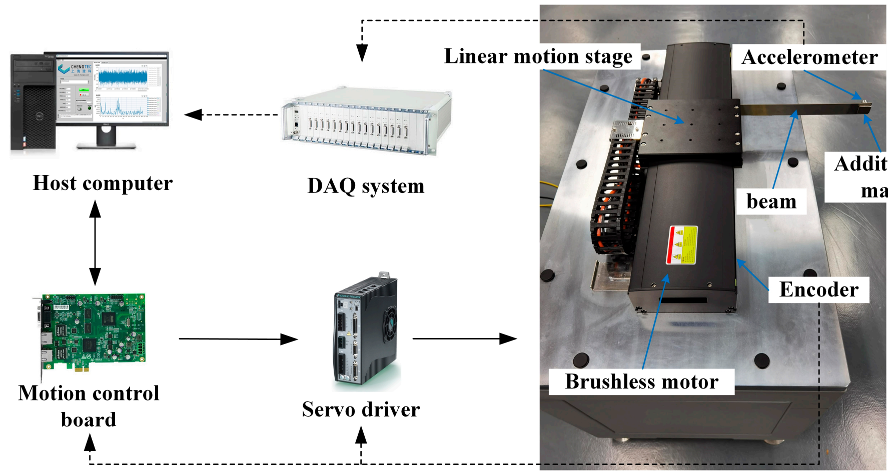

Figure 21. Experimental platform.

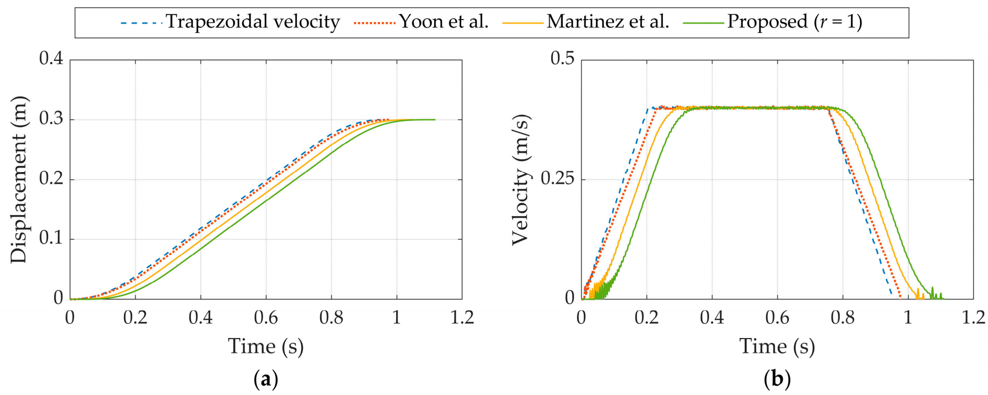

Figure 22. Actual motion profiles of base with different techniques: (**a**) position; (**b**) velocity [16,23].

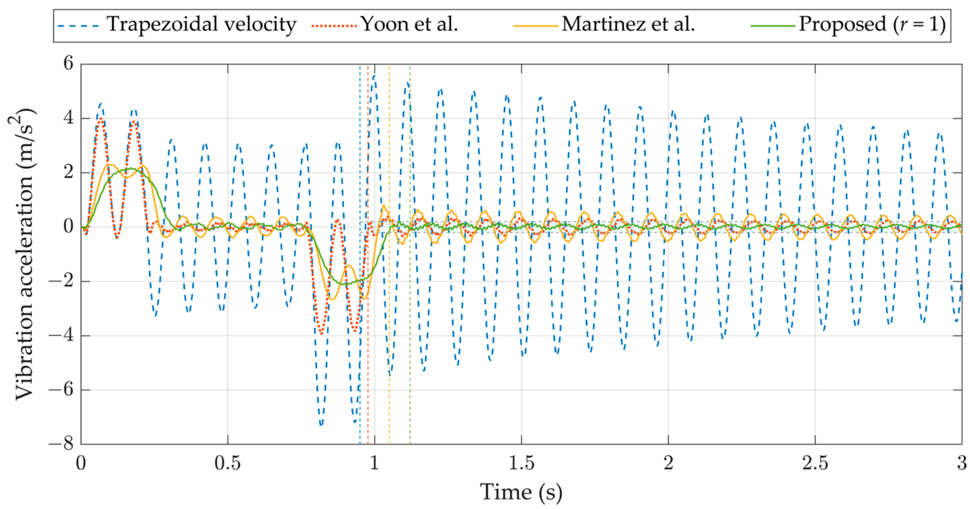

Figure 23. Comparison of vibration accelerations induced by different motion profiles without modeling error [16,23].

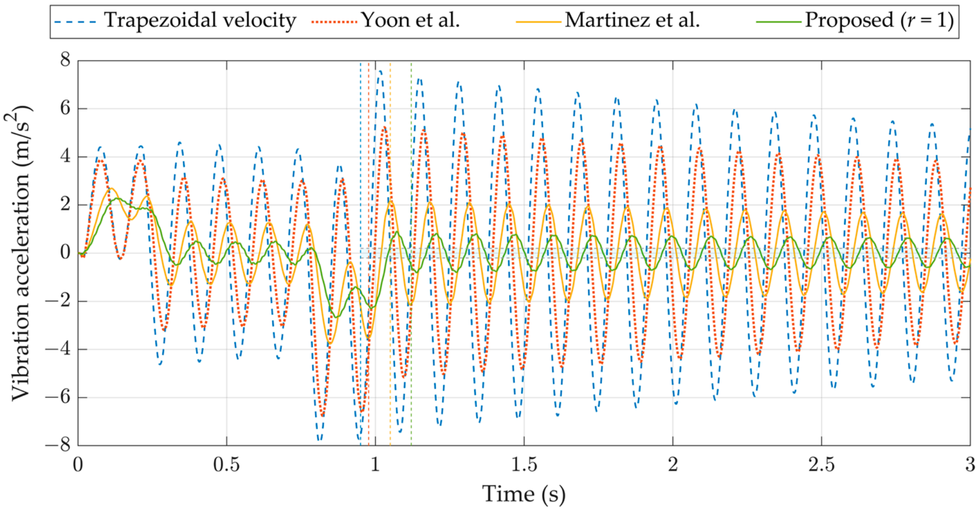

Figure 24. Comparison of vibration accelerations induced by different motion profiles with modeling error [16,23].

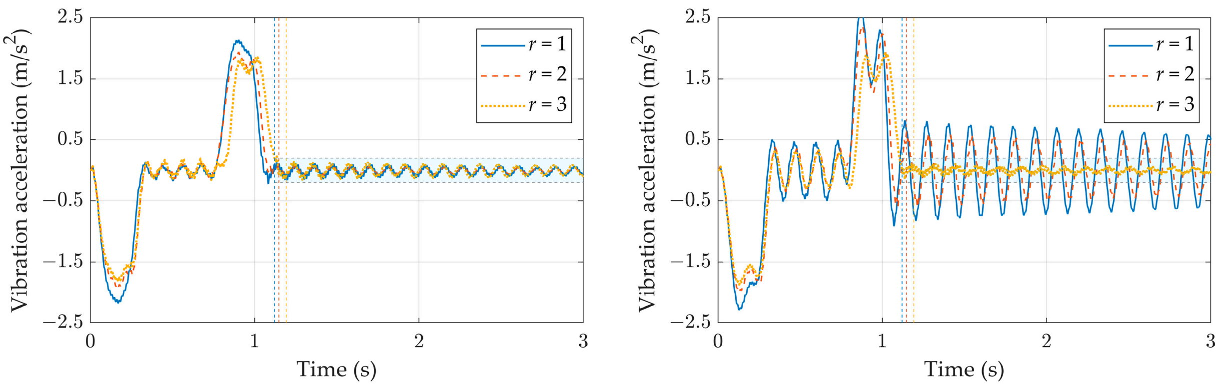

(**a**) Without modeling error (**b**) With modeling error

Figure 25. Comparison of vibration accelerations induced by optimized sinusoidal jerk profiles with different robustness degrees.

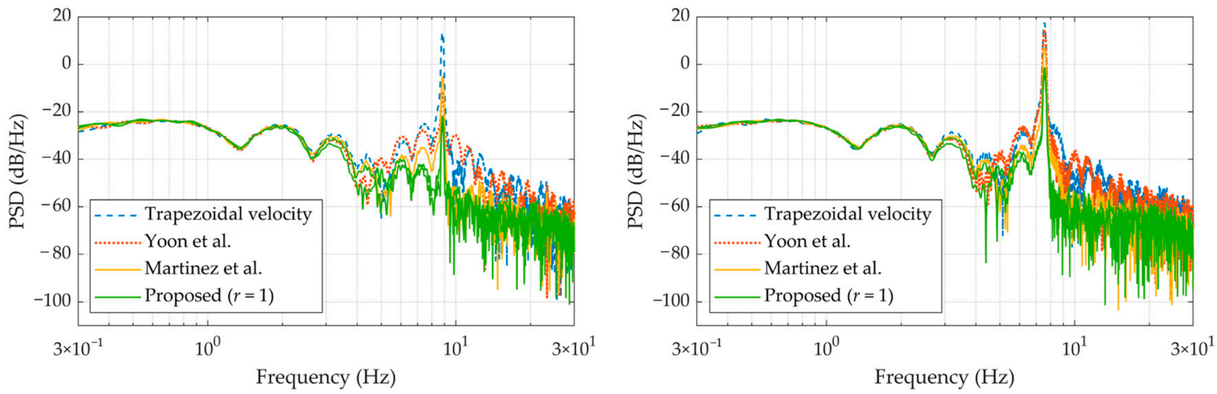

(**a**) Without modeling error (**b**) With modeling error

Figure 26. Power spectral density (PSD) curves of vibration signals induced by different motion profiles [16,23].

Table 9. Experimental comparison results of residual vibrations and settling times induced by different motion profiles.

Motion Profile		Residual Vibration (m/s^2)		Settling Time (s)	
		w/o Modeling Error	w/ Modeling Error	w/o Modeling Error	w/ Modeling Error
Trapezoidal velocity		11.065 (ref)	15.019 (ref)	16.611 (ref)	23.230 (ref)
Yoon et al. [16]		0.720 (−93.5%)	10.386 (−30.9%)	3.653 (−78.0%)	20.733 (−10.8%)
Martinez et al. [23]		1.297 (−88.3%)	4.283 (−71.5%)	6.811 (−59.0%)	16.517 (−28.9%)
Proposed	$r = 1$	0.293 (−97.4%)	1.643 (−89.1%)	**1.121** * (−93.3%)	10.459 (−55.0%)
	$r = 2$	**0.150** * (−98.6%)	1.221 (−91.9%)	1.148 (−93.1%)	7.303 (−68.6%)
	$r = 3$	0.292 (−97.4%)	**0.207** * (−98.6%)	1.192 (−92.8%)	**1.192** * (−94.9%)

* The values in bold indicate the best results achieved among the tested profiles.

From the analysis in Figures 22–26 and Table 9, it is possible to outline the following points:

- Starting with the visual impression in Figure 22, the sinusoidal jerk profile guarantees good smoothness of movement. Due to its continuity up to the jerk level, the adverse influence of high-frequency harmonics can be eliminated;
- As shown in Figure 23, the classic trapezoidal velocity profile, characterized by acceleration discontinuities and infinite jerk, offers the minimum execution time. However, it induces the highest vibration level and, consequently, the longest settling time. By adjusting the acceleration time, the technique in [16] significantly reduced the vibration to 6.5% of the initial level. The proposed sinusoidal jerk profile yields the lowest residual-vibration amplitude, achieving improvements of 59.3% and 77.4% compared to the profiles in [16] and [23] when $r = 1$, respectively;
- The employed profile optimization introduces a slight delay in the reference motion completion time. However, this delay is more than compensated for by the reduced settling time, as the beam reaches a complete standstill state earlier, effectively increasing the operational productivity. The settling time of the proposed profile is identical to the moving time for the nominal case, as the vibration at the end of the motion falls within the specified allowable range;
- It can be seen from the dominant energy peaks in Figure 26a that the vibration mode at 8.81 Hz is mainly excited during the motion. The peak PSD magnitudes obtained using the trapezoidal, modified trapezoidal [16], seven-segment [23], and proposed optimized ($r = 1$) profiles are 13.35 dB, −12.17 dB, −4.77 dB, and −21.80 dB, respectively. Notably, the energy peak is remarkably reduced with the optimized profile, supporting the finding of a more than 90% vibration reduction, as depicted in Figure 23. Moreover, the PSD of the excitation vibration with this profile is smaller than those with the other methods in the high-frequency domain, indicating the smoothness property of the profile;
- In the case of a modeling error, the performance of the proposed profile degrades but still remains superior to the other profiles, as depicted in Figure 24. Increasing the robustness degree (r) can enhance the insensitivity to parameter perturbation. The increment in the settling time due to the modeling error for the optimized profile with the r set to 1 is approximately one order of magnitude, while it remains unchanged with the r set to 3 (Figure 25b);
- While the developed profile demonstrates an outstanding capability of vibration reduction in lightly damped systems, a limitation is that this capability decreases when the damping ratio is significant. Therefore, for future work, it is crucial to improve the profile design by utilizing a complex domain transformation to address damped cases.

On the whole, the obtained experimental results are in good agreement with the numerical results, clearly validating the superiority of the proposed profile optimization method in terms of robust vibration suppression for high-speed machines. This finding is beneficial for substantially enhancing the positioning accuracy and productivity in industrial applications.

6. Conclusions

This paper proposes a novel motion profile design methodology based on a piecewise trigonometric jerk function to address the vibration excitation problem of high-speed machines. The complete analytical mathematical expressions of the motion profile are formulated from the jerk profile. Based on the obtained results, the following conclusions can be drawn:

(1) The motion profile features good smoothness and ensures continuity up to the jerk level. The possibility of introducing physical limits on the velocity, acceleration, and jerk enables the adaptation of the profile to different machines. The critical constraint conditions corresponding to specific cases are derived to obtain the minimum-time solution under physical limitations;
(2) Unlike most previous investigations that focus solely on time optimality as the design metric, this study examined the characteristics of the motion profiles from the perspective of dynamic response in order to take full advantage of the vibration elimination capability inherent in the profiles. The findings highlight the significance of the time durations of specific profile segments, rather than lower jerk values, as the usual manner for motion-induced vibration control;
(3) Based on the established vibration-free conditions, an optimization algorithm is suggested to generate the time–frequency-optimal motion profile such that both the execution time and residual vibration are minimized while respecting the given constraints on the actuator capacities and robustness. The determination of the optimal profile parameters is achieved in an analytical way and does not pose computational difficulties;
(4) A sequence of simulation and experimental tests on a motion stage were carried out to validate the effectiveness of the proposed technique. The results show that the generated velocity, acceleration, and jerk profiles are all bounded and continuous for various given constraint conditions. The comparison studies with other baseline methods demonstrate that the optimized sinusoidal jerk profile exhibits a better performance in terms of vibration reduction and robustness. In particular, it achieves a more than 90% suppression ratio in the residual-vibration amplitude compared to the classical trapezoidal velocity profile. Consequently, the settling time is remarkably shortened, which is beneficial to prevent unnecessary standstill in manufacturing processes. The PSD curves indicate that the high-frequency harmonics are effectively suppressed due to the low-pass filtering effect of the profile;
(5) By adjusting the specified robustness degree, the proposed profiles exhibit high insensitivity to system modeling errors. The optimal profile with threefold vibration mitigation maintains a constant settling time, even if the actual natural frequency deviates by over 10% from its nominal value, for which the motion profile is optimized. This feature makes it suitable for cases in which accurate system parameters are not available.

The application of this newly elaborated motion profile design allows industrial machines to achieve fast and high-precision movements, thereby enhancing both the productivity and task quality. In future work, this profile design will be improved by a complex domain transformation to address damped cases, and the optimization of more types of motion laws will be investigated through an analysis of the vibration characteristics.

Author Contributions: Conceptualization, Y.F.; methodology, Y.F. and Y.Z.; software, Y.F.; validation, G.-N.Z. and Y.Z.; investigation, Y.F. and Y.Z.; resources, C.G.; writing—original draft, Y.F.; writing—review and editing, G.-N.Z. and Y.Z.; supervision, G.-N.Z.; project administration, C.G.; funding acquisition, G.-N.Z. and C.G. All authors have read and agreed to the published version of the manuscript.

Funding: This research was funded by the National Natural Science Foundation of China (grant numbers 62273235, 52105031) and the China Postdoctoral Science Foundation (grant numbers 2022T150407, 2022TQ0209).

Institutional Review Board Statement: Not applicable.

Informed Consent Statement: Not applicable.

Data Availability Statement: The data presented in this study are available on request from the corresponding author. The data are not publicly available due to privacy.

Conflicts of Interest: The authors declare no conflict of interest.

References

1. Iwasaki, M.; Seki, K.; Maeda, Y. High-Precision Motion Control Techniques: A Promising Approach to Improving Motion Performance. *IEEE Ind. Electron. Mag.* **2012**, *6*, 32–40. [CrossRef]
2. Thyer, G.E. *Computer Numerical Control of Machine Tools*; Elsevier: Amsterdam, The Netherlands, 2014; ISBN 1483294617.
3. Verl, A.; Valente, A.; Melkote, S.; Brecher, C.; Ozturk, E.; Tunc, L.T. Robots in Machining. *CIRP Ann.* **2019**, *68*, 799–822. [CrossRef]
4. Biagiotti, L.; Melchiorri, C. *Trajectory Planning for Automatic Machines and Robots*; Springer: Berlin/Heidelberg, Germany, 2008; ISBN 3540856293.
5. Gürocak, H. *Industrial Motion Control: Motor Selection, Drives, Controller Tuning, Applications*; John Wiley & Sons: Hoboken, NJ, USA, 2015; pp. 1–302.
6. Malozyomov, B.V.; Martyushev, N.V.; Sorokova, S.N.; Efremenkov, E.A.; Qi, M. Mathematical Modeling of Mechanical Forces and Power Balance in Electromechanical Energy Converter. *Mathematics* **2023**, *11*, 2394. [CrossRef]
7. Kirgizov, A.K.; Dmitriev, S.A.; Safaraliev, M.K.; Pavlyuchenko, D.A.; Ghulomzoda, A.H.; Ahyoev, J.S. Expert System Application for Reactive Power Compensation in Isolated Electric Power Systems. *Int. J. Electr. Comput. Eng.* **2021**, *11*, 3682–3691. [CrossRef]
8. Berardinis, L.A. Motion Control Gets Gradually Better. *Mach. Des.* **1994**, *66*, 90–93.
9. Kurfess, T.R. *Robotics and Automation Handbook*; CRC Press: Boca Raton, FL, USA, 2005; Volume 414.
10. Heo, H.J.; Son, Y.; Kim, J.M. A Trapezoidal Velocity Profile Generator for Position Control Using a Feedback Strategy. *Energies* **2019**, *12*, 1222. [CrossRef]
11. Yu, Z.; Han, C.; Haihua, M. A Novel Approach of Tuning Trapezoidal Velocity Profile for Energy Saving in Servomotor Systems. In Proceedings of the Chinese Control Conference (CCC), Hangzhou, China, 28–30 July 2015; pp. 4412–4417.
12. Zang, Q.; Huang, J. Dynamics and Control of Three-Dimensional Slosh in a Moving Rectangular Liquid Container Undergoing Planar Excitations. *IEEE Trans. Ind. Electron.* **2015**, *62*, 2309–2318. [CrossRef]
13. Boscariol, P.; Scalera, L.; Gasparetto, A. Nonlinear Control of Multibody Flexible Mechanisms: A Model-Free Approach. *Appl. Sci.* **2021**, *11*, 1082. [CrossRef]
14. Yavuz, Ş.; Malgaca, L.; Karagülle, H. Vibration Control of a Single-Link Flexible Composite Manipulator. *Compos. Struct.* **2016**, *140*, 684–691. [CrossRef]
15. Cusimano, G. Optimized Trapezoidal Acceleration Profiles for Minimum Settling Time of the Load Velocity. *Machines* **2022**, *10*, 767. [CrossRef]
16. Yoon, H.J.; Chung, S.Y.; Kang, H.S.; Hwang, M.J. Trapezoidal Motion Profile to Suppress Residual Vibration of Flexible Object Moved by Robot. *Electronics* **2019**, *8*, 30. [CrossRef]
17. Stretti, D.; Fanghella, P.; Berselli, G.; Bruzzone, L. Analytical Expression of Motion Profiles with Elliptic Jerk. *Robotica* **2023**, *41*, 1976–1990. [CrossRef]
18. Erkorkmaz, K.; Altintas, Y. High Speed CNC System Design. Part I: Jerk Limited Trajectory Generation and Quintic Spline Interpolation. *Int. J. Mach. Tools Manuf.* **2001**, *41*, 1323–1345. [CrossRef]
19. Jeong, S.Y.; Choi, Y.J.; Park, P.G.; Choi, S.G. Jerk Limited Velocity Profile Generation For High Speed Industrial Robot Trajectories. *IFAC Proc. Vol.* **2005**, *38*, 595–600. [CrossRef]
20. Rew, K.H.; Ha, C.W.; Kim, K.S. A Practically Efficient Method for Motion Control Based on Asymmetric Velocity Profile. *Int. J. Mach. Tools Manuf.* **2009**, *49*, 678–682. [CrossRef]
21. Akdağ, M.; Şen, H. Investigation of Performance and Sensitivity of S-Curve Motion Profiles on Reduction in Flexible Manipulator Vibrations. *Arab. J. Sci. Eng.* **2023**, *48*, 12061–12074. [CrossRef]
22. Béarée, R.; Olabi, A. Dissociated Jerk-Limited Trajectory Applied to Time-Varying Vibration Reduction. *Robot. Comput. Integr. Manuf.* **2013**, *29*, 444–453. [CrossRef]
23. García-Martínez, J.R.; Rodríguez-Reséndiz, J.; Cruz-Miguel, E.E. A New Seven-Segment Profile Algorithm for an Open Source Architecture in a Hybrid Electronic Platform. *Electronics* **2019**, *8*, 652. [CrossRef]
24. Meckl, P.H.; Arestides, P.B.; Woods, M.C. Optimized S-Curve Motion Profiles for Minimum Residual Vibration. *Proc. Am. Control Conf.* **1998**, *5*, 2627–2631.
25. Liu, T.; Cui, J.; Li, Y.; Gao, S.; Zhu, M.; Chen, L. Time-Optimal Asymmetric S-Curve Trajectory Planning of Redundant Manipulators under Kinematic Constraints. *Sensors* **2023**, *23*, 3074. [CrossRef]

26. Halinga, M.S.; Nyobuya, H.J.; Uchiyama, N. Generation and Experimental Verification of Time and Energy Optimal Coverage Motion for Industrial Machines Using a Modified S-Curve Trajectory. *Int. J. Adv. Manuf. Technol.* **2023**, *125*, 3593–3605. [CrossRef]
27. Fang, Y.; Qi, J.; Hu, J.; Wang, W.; Peng, Y. An Approach for Jerk-Continuous Trajectory Generation of Robotic Manipulators with Kinematical Constraints. *Mech. Mach. Theory* **2020**, *153*, 103957. [CrossRef]
28. Amthor, A.; Werner, J.; Lorenz, A.; Zschaeck, S.; Ament, C. Asymmetric Motion Profile Planning for Nanopositioning and Nanomeasuring Machines. *Proc. Inst. Mech. Eng. Part I J. Syst. Control. Eng.* **2010**, *224*, 79–92. [CrossRef]
29. Fang, Y.; Hu, J.; Shao, Q.; Qi, J. Fifth Order Trajectory Planning for Reducing Residual Vibration. In Proceedings of the 2019 IEEE 4th International Conference on Advanced Robotics and Mechatronics (ICARM), Toyonaka, Japan, 3–5 July 2019; pp. 999–1004.
30. Lambrechts, P.; Boerlage, M.; Steinbuch, M. Trajectory Planning and Feedforward Design for Electromechanical Motion Systems. *Control Eng. Pract.* **2005**, *13*, 145–157. [CrossRef]
31. Da Rocha, P.A.S.; De Oliveira, W.D.; De Lima Tostes, M.E. An Embedded System-Based Snap Constrained Trajectory Planning Method for 3d Motion Systems. *IEEE Access* **2019**, *7*, 125188–125204. [CrossRef]
32. Bilal, H.; Yin, B.; Kumar, A.; Ali, M.; Zhang, J.; Yao, J. Jerk-Bounded Trajectory Planning for Rotary Flexible Joint Manipulator: An Experimental Approach. *Soft Comput.* **2023**, *27*, 4029–4039. [CrossRef]
33. Li, H.; Le, M.D.; Gong, Z.M.; Lin, W. Motion Profile Design to Reduce Residual Vibration of High-Speed Positioning Stages. *IEEE/ASME Trans. Mechatron.* **2009**, *14*, 264–269.
34. Perumaal, S.S.; Jawahar, N. Automated Trajectory Planner of Industrial Robot for Pick-and-Place Task. *Int. J. Adv. Robot. Syst.* **2013**, *10*, 100. [CrossRef]
35. Valente, A.; Baraldo, S.; Carpanzano, E. Smooth Trajectory Generation for Industrial Robots Performing High Precision Assembly Processes. *CIRP Ann.—Manuf. Technol.* **2017**, *66*, 17–20. [CrossRef]
36. Wu, Z.; Chen, J.; Bao, T.; Wang, J.; Zhang, L.; Xu, F. A Novel Point-to-Point Trajectory Planning Algorithm for Industrial Robots Based on a Locally Asymmetrical Jerk Motion Profile. *Processes* **2022**, *10*, 728. [CrossRef]
37. Wang, Y.; Yang, D.; Gai, R.; Wang, S.; Sun, S. Design of Trigonometric Velocity Scheduling Algorithm Based on Pre-Interpolation and Look-Ahead Interpolation. *Int. J. Mach. Tools Manuf.* **2015**, *96*, 94–105. [CrossRef]
38. Park, B.J.; Lee, H.J.; Oh, K.K.; Moon, C.J. Jerk-Limited Time-Optimal Reference Trajectory Generation for Robot Actuators. *Int. J. Fuzzy Log. Intell. Syst.* **2017**, *17*, 264–271. [CrossRef]
39. Herrera, I.; Sidobre, D. On-Line Trajectory Planning of Robot Manipulator's End Effector in Cartesian Space Using Quaternions. In Proceedings of the 15th International Symposium on Measurement and Control in Robotics, Brussels, Belgium, 8–10 November 2005; pp. 2808–2813.
40. Wang, S.D.; Luo, X.; Xu, S.J.; Luo, Q.S.; Han, B.L.; Liang, G.H.; Jia, Y. A Planning Method for Multi-Axis Point-to-Point Synchronization Based on Time Constraints. *IEEE Access* **2020**, *8*, 85575–85604. [CrossRef]